

University of Mississippi

eGrove

Electronic Theses and Dissertations

Graduate School

1-1-2022

Hot Melt Extrusion (HME) and Amorphous Solid Dispersions (ASDs) Strategies for Poorly Water-Soluble Drugs

Zhiqing Hu

Follow this and additional works at: <https://egrove.olemiss.edu/etd>

Recommended Citation

Hu, Zhiqing, "Hot Melt Extrusion (HME) and Amorphous Solid Dispersions (ASDs) Strategies for Poorly Water-Soluble Drugs" (2022). *Electronic Theses and Dissertations*. 2229.

<https://egrove.olemiss.edu/etd/2229>

This Dissertation is brought to you for free and open access by the Graduate School at eGrove. It has been accepted for inclusion in Electronic Theses and Dissertations by an authorized administrator of eGrove. For more information, please contact egrove@olemiss.edu.

HOT MELT EXTRUSION (HME) AND AMORPHOUS SOLID DISPERSIONS (ASDS) STRATEGIES FOR POORLY WATER-SOLUBLE DRUGS

A Dissertation

Presented in partial fulfillment of requirements

For the Degree of Doctoral of Philosophy in Pharmaceutical Sciences
in the Department of Pharmaceutics and Drug Delivery

School of Pharmacy
The University of Mississippi

By

Zhiqing Hu

May 2022

Copyright Zhiqing Hu 2022

ALL RIGHTS RESERVED

Abstract

Amorphous solid dispersion (ASD) has been well known as a potential strategy to improve the bioavailability and dissolution performance of poorly water-soluble drugs. The primary concern of this approach is the long-term stability of the amorphous drug in the solid dispersion. Accurate prediction and detection of the solubility and miscibility of drugs in polymeric binary systems will be a milestone in the development of ASDs. In Chapter I, a method based on Flory-Huggins (F-H) theory was proposed to predict and calculate the solubility and miscibility of the drug in the polymeric matrix and construct the phase diagram to identify the relevance between drug loading and temperature for ASDs development. For further validation, formulations were developed using HME to verify the accuracy of the phase diagram and to get in the hot-melt extrusion (HME) process design space and optimization. Chapter II aimed to investigate the impacts of HME processing parameters by the design of experiment (DoE) for the poorly water-soluble compound. This study presents a simple, novel, and three-level factorial design to evaluate each condition's effect and explore the optimized formulation. Barrel temperature and screw speed were the most affected parameters in this research. The primary objective of Chapter III was to combine fused deposition modeling (FDM) 3D printing with HME technology to explore the effect of manufacturing tablets with different densities and designs. These tablets are designed with an outer shell and inner core. HME technology causes some crystalline drugs to change form into an ASD during the processes used. Overall, this work illustrated the impacts of changing a printed tablet's filling density as a strategy to control the drug release performance for 3-dimensional (3D) printed dosages and the possibility of HME coupling 3D printing technology to prepare ASDs.

List of Abbreviations

ASD: amorphous solid dispersion

HME: hot melt extrusion

Indo: indomethacin

PVP VA 64: polyvinyl pyrrolidone vinyl acetate

Kollidon[®] VA 64: polyvinyl pyrrolidone vinyl acetate

F-H theory: Flory-Huggins theory

G-T equation: Gordon- Taylor equation

BCS: biopharmaceutical classification system

DSC: differential scanning calorimetry

TGA: thermogravimetric analysis

Eq: equation

χ : interaction parameter

T_g: glass transition temperature

T_{gmix}: ASDs glass transition temperature

T_{g1}: drug glass transition temperature

T_{g2} : polymer glass transition temperature

w_1 : drug weight fraction

w_2 : polymer weight fraction

ϕ : drug volume fraction

ϕ_{polymer} : polymer volume fraction

$1-\phi$: polymer volume fraction

ρ_1 : drug density

ρ_2 : polymer density

K : adjustable fitting parameter

T_m : melting point temperature

ΔG_{mix} : Gibb's free energy of mixing

ΔH_{mix} : the change in enthalpy

ΔS_{mix} : the change in entropy

δ_t : solubility parameter

δ_d : components of disperse forces

δ_p : components of polar group forces

δ_h : components of hydrogen bond energy

F_{di} : group contribution to the disperse forces,

E_{hi} : group contribution to hydrogen bonding energy

F_{pi} : plane symmetry factor of polar groups

V_0 : group contributions to the molar volume

R^2 : R-squared

GFA: glass forming abilities

MPD: melting point depression

UCST: upper critical solution temperature

T_{min} : minimum processing temperature

GI fluids: gastrointestinal fluids

PM: physical mixture

T_{deg} : degradation temperature

XRD: X-Ray Diffraction

PXRD: Powder X-Ray Diffraction

θ : theta

RH: relative humidity

FDA: Food and Drug Administration

EMA: European Medicine Agency

QbD: Quality by Design

PAT: process analytical technology

API: active pharmaceutical ingredient

ΔG_{mix} : Gibb's free energy of mixing

R^2 : R square

PM: physical mixture

DoE: Design of Experiments

RSD: response surface design

CCD: central composite design

HCl: Hydrochloric acid

HPLC: High-performance liquid chromatography

3D: 3-dimensional

TA: texture analysis

SEM: Scanning electron microscope

FDM: Fused deposition modeling

USP: United States Pharmacopeia

PLA: Polylactic acid

HPMC: Hydroxypropyl methylcellulose

HPMCAS: Hypromellose acetate succinate

CAD: Computer-aided design

AM: Additive manufacturing

ACKNOWLEDGMENT

I have been on an exciting, but difficult journey to obtain a Ph.D. and I would not have succeeded without all the wonderful support and help I've received along the way. I would like to thank each and every person who has provided mentoring, love, advice, or even the smallest of kindnesses.

First and foremost, I would like to thank my advisor, Dr. Michael A. Repka, for everything he did for me over the last 5 years. He taught me so much and always went above and beyond whenever I needed him. He is a wonderful professor and a dear friend. His insightful suggestions always pushed me forward and brought my work to a higher level.

I would also like to thank my committee members, Dr. Chalet Tan, Dr. Seong Bong Jo, and Dr. Samir Anis Ross, for all their valuable guidance and advice throughout my dissertation.

I would also like to give a special thank you to my colleagues at Biogen for their wonderful collaboration. The time spent among them not only furthered my understanding of research and development, but also my appreciation for strong teamwork and a great work ethic.

I am so very grateful for all the people who helped me this long way. I want to thank all my friends and lab mates, for their company and the excellent environment they provided where we could both improve academically and socially. The time we spent together was pleasant and unforgettable.

In addition, I would like to thank my parents and my boyfriend for their unlimited love and trust all the time. It is their encouragement that helped me make it through the hardest times and made the sweetest times even sweeter.

TABLE OF CONTENTS

ABSTRACT	ii
LIST OF ABBREVIATIONS	iii
ACKNOWLEDGMENT.....	viii
TABLE OF CONTENTS.....	x
LIST OF TABLES	xv
LIST OF FIGURES	xvi
PREFACE	xix
CHAPTER I	1
1.1. Introduction	1
1.2. Materials and Methods	4
1.2.1. Materials	4
1.2.2. Sample Preparation	4
1.2.3. Drug and Polymer Thermal Stability Analysis.....	4
1.2.4. Glass Forming Abilities (GFA).....	5
1.2.5. Melting Point Depression (MPD) Method.....	5

1.2.6. Theoretical Considerations.....	6
1.2.7. Prediction of Solubility/Miscibility Using Drug and Polymer Solubility Parameters.....	9
1.2.8. Application of phase diagram for HME Process map.....	10
1.2.9. Preparation of Amorphous Solid Dispersions through Hot Melt Extrusion: validation of the phase diagram.....	10
1.2.10. Stability Analysis.....	11
1.2.11. X-Ray Diffraction (XRD) analysis.....	11
1.3. Results and discussions	12
1.3.1. Glass Forming Abilities (GFA).....	12
1.3.2. Drug-Polymers Miscibility Prediction by Solubility Parameters	12
1.3.3. Melting Point Depression	13
1.3.4. Construction of the Phase Diagram.....	16
1.3.5. HME Process Design Space.....	18
1.3.6. Preparation of ASDs by HME: validation of the phase diagram.....	20
1.3.7. Accelerated stability test by PXRD.....	21
1.4. Conclusion.....	23

CHAPTER II.....	24
2.1. Introduction	24
2.2. Materials and Methods	28
2.2.1. Materials	28
2.2.2. Physical Mixture (PM) Preparation	28
2.2.3. Rheology Studies	28
2.2.4. Design of Experiment (DoE).....	29
2.2.5. Preparation of Amorphous Solid Dispersions through Hot Melt Extrusion	31
2.2.6. Dissolution Studies	32
2.2.7. Analysis of Storage Stability	33
2.2.8. X-Ray Diffraction (XRD) analysis.....	33
2.3. Results and Discussions	34
2.3.1. Rheology Studies of Indo-Kollidon [®] VA 64 System	34
2.3.2. Hot melt extrusion parameters optimization by DoE	37
2.3.3. Hot-melt Extrusion and Preparation of Indo-Kollidon [®] VA 64 ASDs: Validation for DoE optimization	39

2.3.4. Dissolution studies.....	41
2.3.5. Accelerated stability test of Indo-Kollidon® VA 64 ASDs by PXRD....	43
2.4. Conclusion	45
CHAPTER III	46
3.1 Introduction	46
3.2 Materials and Methods	48
3.2.1. Materials	48
3.2.2. Formulations.....	49
3.2.3. Hot melt extrusion (HME) Process.....	49
3.2.4. Filaments Texture Analysis (TA).....	50
3.2.5. Differential Scanning Calorimetry (DSC).....	51
3.2.6. 3D Printing.....	51
3.2.7. X-Ray Diffraction (XRD) Analysis.....	53
3.2.8. Scanning Electron Microscopy (SEM)	53
3.2.9. Tablets Physical Parameters	53
3.2.10. In Vitro Drug Release Study.....	54

3.2.11. Dissolution Mathematical Model Study.....	54
3.3. Results and Discussions	57
3.3.1. Thermal Analysis	57
3.3.2. X-Ray Diffraction (XRD) Analysis.....	58
3.3.3. Filament Texture Analysis.....	58
3.3.4. Tablets Morphology Analysis.....	59
3.3.5. In Vitro Drug Release Study.....	61
3.3.6. Analysis of the Drug Release Using Mathematical Models.....	62
3.4 Conclusions	65
Reference	66
VITA.....	80

LIST OF TABLES

Table 1.1. HME processing parameters with physical appearances.....	20
Table 2.1. DoE CCD Design for the experiments.....	30
Table 2.2. HME processing parameters and physical-chemical characterizations of optimization design.....	39
Table 3.1. Formulation composition for extrusion.....	49
Table 3.2. Density gradient modification 3D Printing tablets design.....	52
Table 3.3. Filament's stiffness test results.....	59
Table 3.4. Geometric characteristics and textural properties of the 3D printed tablets.....	60
Table 3.5. Dissolution kinetic parameters of 3D printing tablets.....	63
Table 3.6. R/F parameters for T1-T9 fitted by Peppas-Sahlin model.....	65

LIST OF FIGURES

Figure 1.1. Chemical Structure of (a) Indomethacin; (b) Kollidon [®] VA 64	4
Figure 1.2. Indo-Kollidon [®] VA 64 DSC thermograms overlay. (a) Melting point depression from the 1st heating ramp. (b) ASDs T _g Overlay from the 2nd heating ramp	14
Figure 1.3. Indo- Kollidon [®] VA 64 ASDs T _g of the mixture by DSC (triangle) and G-T equation prediction (solid line)	15
Figure 1.4. (a) F-H interaction parameter plot close to the Indo melting point. (b) Indo-Kollidon [®] VA 64 system $\Delta G_{\text{mix}}/RT$ as a function with drug volume fraction.....	15
Figure. 1.5. Gibb's free energy of mixing/RT as a function of Indo volume fraction for model compound and Kollidon [®] VA 64 system at 25, 50, 80, 100, 120, 140, and 160 °C.....	16
Figure 1.6. Indo- Kollidon [®] VA 64 binary system phase diagram.....	18
Figure 1.7 The temperature-composition phase diagram for HME process design space application.....	19
Figure 1.8. XRD overlay for ASDs formulation (F1-F6) at Tzero and 1month under 40 °C/ 75% RH stability chamber.....	22
Figure 2.1. Instruction of Quality by design (QbD)	27
Figure 2.2. Chemical Structure of (a) Indomethacin; (b) Kollidon [®] VA 64.....	28

Figure 2.3. The complex viscosity of Indo-Kollidon® VA 64 PM under the temperature ramp at 0.1 rad/s ang. Frequency.....	34
Figure 2.4. The complex viscosity of Indo-Kollidon® VA 64 PM under the dynamic frequency sweep at 160 °C temperature	35
Figure 2.5. The predicted miscibility limitation of the Indo-Kollidon® VA 64 PM at 160 °C by zero shear viscosity method.....	37
Figure 2.6. Prediction profiler for the DoE Response Surface Analysis.....	39
Figure 2.7. Dissolution profiles of indomethacin released from the extrudates powder and of the pure Indo.....	42
Figure 2.8. XRD overlay for ASDs formulation (F1-F5) PM and after one month under 40 °C/ 75% RH stability chamber.....	44
Figure 3.1. Figure 1. Standard screw configuration of Thermo Scientific™ Pharma 11 Twin-screw Extruder.....	50
Figure 3.2. PLA texture analysis test.....	51
Figure 3.3. 3D printing design.....	52
Figure 3.4. Figure 4. DSC thermogram for F1 (Core) and F2 (Shell) homogeneous mixture and the printed core and shell ground powder.....	57
Figure 3.5. XRD overlay of F1 and F2.....	58

Figure 3.6. SEM 3D structure of T5, with a 30% shell fill and 50% core fill, (a) top view of the shell (b) top view of the core (c) side view of the core, and (d) side view of the shell..... 60

Figure 3.7. In vitro drug release profiles of tablets T1-T9.....62

PREFACE

This dissertation has been prepared in manuscript formats.

Manuscript I: Prediction and Construction of Drug-Polymer Binary System Thermodynamic Phase Diagram in Amorphous Solid Dispersions (ASDs)

Manuscript II: Design of Experiment (DoE) in hot-melt extrusion (HME) process for amorphous solid dispersions (ASDs) formulation optimization

Manuscript III: Development of Controlled Release Oral Dosages by Density Gradient Modification via Three-Dimensional (3D) Printing and Hot-Melt Extrusion (HME) Technology

CHAPTER I

PREDICTION AND CONSTRUCTION OF DRUG-POLYMER BINARY SYSTEM THERMODYNAMIC PHASE DIAGRAM IN AMORPHOUS SOLID DISPERSIONS (ASDS)

1.1. Introduction

Developing amorphous solid dispersions has become an attractive strategy for improving compound solubility, dissolution rate, and oral bioavailability [1-4]. The aqueous drug solubility can be significantly increased once combined into a dispersed system than in its crystalline form. However, the Gibbs free energy is higher for the amorphous state than in the crystalline state, so the amorphous drugs usually have long-term stability concerns and challenges because of the quick recrystallization tendency during processing and storage [5-7]. There are many ways to improve the stability of amorphous drugs, such as selecting proper polymeric carriers and proper drug loading for the formulation, allowing the drug to disperse into the polymeric matrix, and forming a stable amorphous solid dispersion [8]. Therefore, there is an urgency to develop a method to select the suitable polymer and the optimum drug loading that could help the stabilization of the ASD formulation [7].

Even though ASD can help improve the solubility of poorly water-soluble drugs, the selection of polymer type is essential to stabilize the high-energy nature of ASD. The miscibility of a drug and a polymer system is crucial since the specific interaction between the drug and

polymer is critical for the stability of the ASD system. Another critical factor that needs to be considered when producing ASD formulation is the amount of drug loading integrated into the polymeric matrix. High drug loading can cause instability of the dispersion system and further recrystallization, which leads to solubility reduction [9].

Developing a one-phase drug-polymer binary system requires the two components (drug and polymer) to be thermodynamically miscible; also, the process parameters need to be optimized during this production [10]. The most common methods to prepare ASDs are hot-melt extrusion (heat-based) and spray drying (solvent-based) in the pharmaceutical industry [3]. Furthermore, since the preparation of ASDs may occur at non-ambient temperatures or in the presence of organic solvents, disturbance of the system during operation can guide a dynamic system that re-equilibrates after processing [11]. A more relevant and logical approach would be beneficial to comprehend the miscibility degree of a drug in a polymeric matrix as a function of temperature and how this might be connected to the molecular structure and physical characteristics of the drug-polymer combination. [12,13]. It would be contributory to identifying better drug-polymer compositions that form strong interactions between them by implementing simple experimental methods. The construction of a phase diagram could guide the selection of ideal drug loading and optimize processing conditions to maximize the stability of the ASD formulation [11,14,15].

HME has been extensively explored as one of the development strategies for preparing ASDs, which improves the solubility and bioavailability of poorly water-soluble drugs (BCS Class II and Class IV). HME is an application that combines mixing, melting, softening, and conveying simultaneously. The optimization of the HME process in the pharmaceutical area has been investigated by formulation development, process parameters, and other factors [2,7].

In the present study, the melting point depression method was evaluated using DSC measurements based on the Flory-Huggins (F-H) theory, in which the F-H interaction parameter (χ) could be determined from the mixture of different combinations of drug and polymer systems [12,16,17]. Recent studies reported that χ is not only drug loading dependent but also temperature-dependent [18-20]. Gibb's free energy of mixing (ΔG_{mix}) was not favorable when χ was positive, indicating immiscibility between the drug-polymer system. Conversely, when χ had a negative or slightly positive value, the ΔG_{mix} was negative, implying that the drug and polymer system was miscible. This research will allow for a better understanding of F-H interaction theory for drug-polymer miscibility suggestions to explore more about the thermodynamics behavior of drug-polymer mixing during processing and the choice and loading limit of the drug and polymeric carrier in future studies. This research aimed to build and construct these diagrams that provide thermodynamics information through different processing conditions, including the relationship between drug loading, temperature, and phase transitions and separation. This binary phase diagram allows for predicting the solubility and miscibility of different drug-polymer systems [16,18]. Building phase diagrams that significantly correlate with experimental measurements and product states would benefit formulation development studies [13,14].

The acquired data will guide the HME design space map for extruded ASDs preparation. Additionally, the study aimed at providing a logical and reasonable discussion on how this phase diagram can be used to evaluate the appropriate drug for the ASD system. [21,22]. Also, validated the prediction from the phase diagram by executing the HME based on the suggested information and utilized phase diagram validation to evaluate the stability analysis. The model drug selected in this investigation was indomethacin (Indo), a BCS Class II (low solubility, high permeability) compound, and Kollidon[®] VA 64 was chosen as a polymeric carrier for ASDs.

1.2. MATERIALS AND METHODS

1.2.1. Materials

Indomethacin was purchased from TCI (Tokyo Chemical Industry Co., Ltd., Tokyo, Japan); Kollidon[®] VA 64 grade was gifted from BASF (Florham Park, NJ, USA). The chemical structure of the indomethacin and Kollidon[®] VA 64 are shown in Figure 1.1.

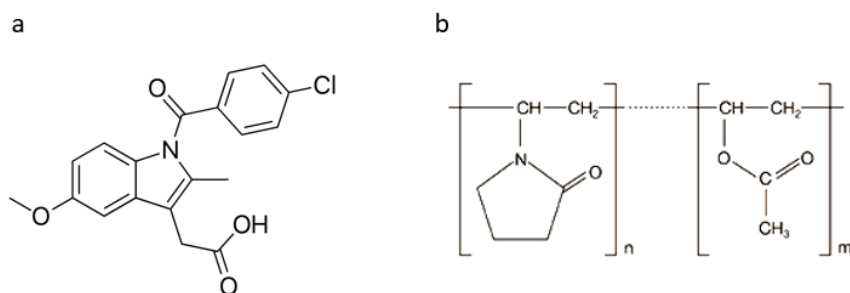


Figure 1.1. Chemical Structure of (a) Indomethacin; (b) Kollidon[®] VA 64.

1.2.2. Sample Preparation

Indomethacin and Kollidon[®] VA 64 were stored in a vacuum drying oven at 40 °C, 200 mbar, at least two days before further investigation. Then, different drug loading 10, 20, 30, 40, 50, 60, 70, 80, and 90% (w/w) were mixed with Kollidon[®] VA 64 using MaxiBlend[™] blender (GlobePharma Inc, New Brunswick, NJ, USA) at 30 RPM for 10 min to ensure an even distribution of chemicals (total weight 10.0 g per batch).

1.2.3. Drug and Polymer Thermal Stability Analysis

DSC and TGA tests were performed to verify the drug and polymer thermal stability and provide information about their physical state and thermal behavior for future analysis. For the

DSC test, TA DSC 25 (TA Instruments, New Castle, DE, USA) was used in this research. Around 5 mg of each drug/polymer physical mixture with a different drug loading was packed into a T_{zero} hermetic aluminum pan (TA Instruments, Waters, LLC, USA) with a lid. A pinhole was made into the lid to allow the moisture to escape. DSC was conducted at a heating rate of 10 °C/min from 0°C to 200°C. For the TGA test, approximately 5-10 mg drug/polymer were placed in a platinum pan with a heating rate of 10 °C /min from 25°C to 200 °C to check the sample weight loss with the heating flow. Nitrogen was used as the purge gas for both tests.

1.2.4. Glass Forming Abilities (GFA)

GFA is a classification system based on drugs recrystallization behavior during DSC heat-cool-heat cycles. GFA Class 1 defines drugs that will recrystallize at a cooling section with a cooling rate of 20 °C/min; GFA Class 2 includes drugs that will recrystallize at the 2nd heating ramp with the heating rate 10 °C/min. While Class 3 drugs will not recrystallize either at a 20 °C/min cooling rate or the 10 °C/min 2nd heating ramp [24,25]. This GFA classification system allows for more understanding of the glass-forming behavior of drugs and guides to making better suitable drugs for ASD development with long-term stability.

1.2.5. Melting Point Depression (MPD) Method

Modulated DSC (mDSC) was used for the MPD method, where nitrogen was used as the purge gas. The modulation amplitude applied over the entire method was 1 °C every 60 s for mixtures of Indo and Kollidon[®] VA 64. Around 5 mg sample was packed into a T_{zero} pan (TA Instruments, Waters, LLC, USA) with a lid. A pinhole was made in the lid to allow the moisture to escape. An initial drying step with a heating rate of 10 °C/min to 80 °C was used to remove residual moisture from the system before the heat-cool-heat cycle since the moisture could

interfere with the DSC heat flow measurements. DSC was set up after the initial heat cycle to equilibrate at 0 °C for 5 min. Melting depression experiments were conducted at a heating rate of 2 °C/min from 0°C to 200 °C and allowed to re-equilibrate for 5 min to make sure the compound and polymer are melted; followed by a jump cooling step to 0 °C, then isothermal step for 5 min again. The DSC pans were then reheated at 2 °C /min to 200 °C. The start point of the endothermic melting peak (T_m onset) was computed by the Trios software (TA Instruments, Waters, LLC, USA) and used for the calculation in this research.

This heat-cool-heat cycle was performed as mentioned above to identify the T_m and T_g of drug-polymer solid dispersion. T_m was estimated from the 1st heating ramp and the T_g from the 2nd heating ramp. This T_g value represented the neat T_g of freshly prepared ASDs when only a single T_g appeared in this section.

1.2.6. Theoretical Considerations

From the Gordon-Taylor (G-T) equations (Eqs 1, and 2), if the drug-polymer is miscible, there should only be a single T_g for this binary system, and this T_g value can be predicted by the equation below:

$$T_{gmix} = \frac{(w_1 T_{g1} + K w_2 T_{g2})}{(w_1 + K w_2)} \quad (1)$$

$$K = \rho_1 T_{g1} / \rho_2 T_{g2} \quad (2)$$

Where, T_{gmix} , T_{g1} , and T_{g2} are the glass transition temperature of ASDs, pure drug, and pure polymer, respectively; w_1 and w_2 are the drug and polymer weight fraction, respectively; ρ_1 and ρ_2 are the drug and polymer density, respectively; K is the adjustable fitting parameter calculated by drug and polymer densities and T_g .

According to F-H theory, the change in Gibb's free energy of mixing for drug-polymer binary solid dispersions can be described as below (Eq 4):

$$\Delta G_{mix} = \Delta H_{mix} - T * \Delta S_{mix} \quad (3)$$

Where, ΔG_{mix} , ΔH_{mix} , and ΔS_{mix} are the change in Gibb's free energy of mixing, enthalpy, and entropy, T represents temperature in kelvin.

Then, Gibb's free energy of mixing can be calculated by F–H drug-polymer interaction parameter, χ as shown in Eq 4.

$$\frac{\Delta G_{mix}}{RT} = \varphi \ln \varphi + \frac{(1-\varphi)}{m} \ln(1 - \varphi) + \varphi(1 - \varphi)\chi \quad (4)$$

Where φ , and $1-\varphi$ are the volume fraction of drug and polymer, respectively. χ is the F-H interaction parameter, R is the molar gas constant, T is the temperature in kelvin, m is the ratio of the volume of a polymer chain to drug molecular volume, and the following equation can calculate it

$$m = \frac{\frac{M_{W2}}{\rho_2}}{\frac{M_{W1}}{\rho_1}} = \frac{M_{W2} * \rho_1}{M_{W1} * \rho_2} \quad (5)$$

M_{w1} and M_{w2} are the molecular weights of drug and polymer, respectively, and ρ_1 and ρ_2 are the densities of drug and polymer. ΔG_{mix} can be calculated by Eq 4. at a specified temperature and the corresponding interaction parameter. MPD DSC data from the different compositions can be used to predict the interaction parameter using the following equation (Eq 6):

$$\frac{1}{T_m} - \frac{1}{T_{m0}} = -\frac{R}{\Delta H} \left[\ln \varphi + \left(1 - \frac{1}{m}\right) (1 - \varphi) + \chi(1 - \varphi)^2 \right] \quad (6)$$

Where T_m and T_{m0} are the melting points of the drug crystal in the drug/polymer physical mixture and the pure drug, respectively, and ΔH is the heat of fusion of the drug. It should be noted that the interaction parameter χ is not constant but temperature and composition dependent. To develop a phase diagram to accommodate temperature variation, it defines the temperature dependence of the F-H interaction parameter χ as shown in Eq 7 below:

$$\chi \cong A + \frac{B}{T} \quad (7)$$

where A is the value of the temperature-independent term for entropic contribution, and B is the value of the temperature-dependent term for enthalpy contribution; the relationship has been simplified as this equation and has proven to be sufficient in many drug-polymer systems exhibiting an upper critical solution temperature (UCST). The first-order relationship between χ and $1/T$ has been used to extrapolate the value of χ for drug-polymer binary systems outside experimental temperatures. In this study, we have employed this equation that relates χ to temperature and used this to identify F-H constants A and B. Suppose the relationship between χ and T within a given temperature range can be determined for specific drug-polymer binary systems. In that case, ΔG_{mix} versus composition and temperature may be constructed by combining Eqs 4, 6, and 7. Furthermore, the maximum drug-polymer miscibility boundary (spinodal curve) may be calculated by determining the second derivative of the free energy (Eq 7) and setting it equal to zero, as shown in Eq 8 below:

$$\frac{1}{\varphi_{drug}} + \frac{1}{m^*\varphi_{poly}} - 2\chi_{drug-poly} = 0 \quad (8)$$

Where the interaction parameter χ can be substituted from Eq 7, thereby, the maximum drug-polymer miscibility curve may be obtained.

1.2.7. Prediction of Solubility/Miscibility Using Drug and Polymer Solubility Parameters

In this research, the Van Krevelen group contribution method [28] has been used to calculate the solubility parameter δ_t of indomethacin and the polymer, which may be expressed as Eq 9:

$$\delta_t = \sqrt{\delta_d^2 + \delta_p^2 + \delta_h^2} \quad (9)$$

Where δ_d and δ_p and δ_h are the components of disperse forces, polar group forces, and hydrogen bond energy, respectively, these forces can be calculated as follows Eqs 10, 11, and 12.

$$\delta_d = \frac{\sum F_{di}}{V} \quad (10)$$

$$\delta_p = \frac{\sum F_{pi}^2}{V} \quad (11)$$

$$\delta_h = \sqrt{\frac{\sum E_{hi}}{V}} \quad (12)$$

F_{di} is the group contribution to the dispersed forces, E_{hi} is the group contribution to hydrogen bonding energy, and F_{pi} is the plane symmetry factor of polar groups. The values of F_{di} , F_{pi} , and E_{hi} of each group at 25 °C used in this work were chosen from Van Krevelen's solubility parameters [28].

Therefore, the drug-polymer interaction parameter χ may be calculated as follows [28].

$$\chi = \frac{V_0}{RT} (\delta_{drug} - \delta_{polymer})^2 \quad (13)$$

Where V_0 is the group contributions to the molar volume, the volume of the lattice site, and the molar volumes of a single polymer unit calculated from the group contributions were used for the polymer-drug system. As shown in Eq 13, χ refers to the square of the difference in solubility

parameters calculated from the values of group contributions at 25 °C. The drug-polymer interaction parameters for the Indo-based systems as calculated from solubility parameters (group contribution method) compared with the results obtained from the melting point depression method.

1.2.8. Application of phase diagram for HME Process map

The composition temperature phase diagram based on the F-H theory introduced before can also be applied to the HME to understand further and optimize the formulation performance and process development. The process design space that needs to be constructed is bounded by the drug-polymer solubility curve and the drug-polymer thermal degradation range [29]. Polymer T_g and the minimum processing temperature (T_{min}) were also introduced to the design map to provide the viscosity requirements- with the lower drug loading- for the process; It was reported that most polymers need at least 10 °C above the polymer T_g (usually 10-15 °C above T_g) to ensure the drug will be molten [30,31].

1.2.9 Preparation of Amorphous Solid Dispersions through Hot Melt Extrusion: validation of the phase diagram

For further investigation on the impacts of processing temperature and other factors on extruded filaments' characteristics, ASDs were prepared by HME for validation. The HME processing conditions are clearly suggested previously from the temperature-composition phase diagram, which implies the temperature should be above T_{min} (around 120 °C) and under T_{deg} (about 200 °C). Amorphous solid dispersions of 20% and 40% drug loading of indomethacin in Kollidon® VA 64 were selected for investigation. The physical mixtures (PM) of Indo and

Kollidon[®] VA 64 (entire batch of 100 g) were prepared at the weight ratios and thoroughly blended for 30 min at 30 RPM by MaxiBlend[™] blender (GlobePharma Inc, New Brunswick, NJ, USA).

The ASDs were prepared by a Thermo Scientific[™] Pharma 11 Twin-screw Extruder (Thermo Fisher, Waltham, MA, USA). The standard screw configuration with four conveying zones and three mixing zones was used in this study, and 100 g batch sizes of PM with the screw rate of 20 RPM were set for the whole extruding process. The extruding temperatures were set between 120 °C and 170 °C. For the examination, the torque and physical appearance of the filaments were also recorded.

1.2.10 Stability Analysis

The extruded filaments produced by the HME process earlier were milled by mortar and pestle into powder after it was allowed to cool down. The storage stability testing was evaluated under accelerated testing conditions at 40 °C and 75% relative humidity (RH) for a month. XRD was used to evaluate the structural states of the extruded samples.

1.2.11 X-Ray Diffraction (XRD) analysis

PXRD evaluated the milled extrudates' physical state at zero time point (T_{zero}) and after one month. The investigation was pursued by the D8 ADVANCE ECO diffractometer (Bruker, Billerica, MA, USA). The spectra were collected from the scans within the range of 0.0 ° to 40.0 ° at 2-Theta (2θ) with a 0.01 ° step size and 1 s per step time.

1.3. Results and discussions

1.3.1. Glass Forming Abilities (GFA)

Applying the DSC method described above, Indo is classified as class 3 by the GFA definition. It suggests that indomethacin is suitable for ASD development since it will not recrystallize easily neither in the first cooling cycle or the 2nd heating ramp. It will also be beneficial to the ASD formulation's long-term stability. The following studies will further emphasize this result, as discussed below.

1.3.2. Drug-Polymers Miscibility Prediction by Solubility Parameters

Solubility parameters of drugs and polymers were estimated using the Hoftyzer and Van Krevelen method with the information provided in Table 1 [23]. The solubility parameter values obtained for Kollidon[®] VA 64 was 21.1 MPa^{1/2}, and indomethacin solubility parameters were calculated for 23.38 MPa^{1/2}. Therefore, the drug-polymer interaction parameter χ calculated by equation 13 is 0.5654, slightly above zero. However, since the value is for all compositions ranges, it still suggested that the indomethacin and Kollidon[®] VA 64 were miscible.

Solubility parameters here were used to suggest drug-polymer miscibility information. It is well-known that compounds with similar solubility parameters (~ 7 MPa^{1/2}) are more likely to be miscible. On the other hand, compounds with solubility parameters differing by more than 10 MPa^{1/2} are more likely to be immiscible [24]. In this research, the difference between the solubility parameter of indomethacin and Kollidon[®] VA 64 was 2.28 MPa^{1/2} which is less than 7 MPa^{1/2}. This value suggests that indomethacin is miscible with Kollidon[®] VA 64. Further thermal analysis should be conducted to examine the possibility of glass-forming ability.

1.3.3. Melting Point Depression

The Indo and Kollidon[®] VA 64 TGA thermogram showed less than 0.5% weight loss of the pure powder after drying the sample for two days, followed by heating to 200 °C. This result verified the drug and polymer's thermal stability and confirmed the MPD method's possibility by the DSC heating ramp below.

Usually, the melting point of solid crystalline compounds is highest when the substance is pure, and T_m is depressed in impure solids. In this research, Indo showed melting point depression with the Kollidon[®] VA 64 as a polymeric carrier across the compositions range, as demonstrated in Figure 1.2a. DSC was employed to understand the miscibility between Indo and Kollidon[®] VA 64 and suggest the optimum drug loading choice for stabilizing the dispersion. Previously, it has been reported that the solubility of a drug within a polymeric matrix can be determined by measuring melting temperatures (T_m onset from DSC 1st heating ramp) of known different drug-polymer compositions [16, 17]. The T_m onset was explored to reflect the dissolution of several drug compositions in this research.[18]. On the addition of the polymer, MPD occurred relative to the T_m of indomethacin. $(\frac{1}{T_m} - \frac{1}{T_{mo}})$, can be used with Eq 6 [20]. Indo T_m onset decreased with increasing the fraction of Kollidon[®] VA 64 used, as shown in Figure 1.2a. From Fig 1.2b, the endothermic melting peak shown in 1st heating ramp was gone after the rapid cooling, and it only showed one T_g for the system of all drug-polymer compositions (10-90%). The DSC heat-cool-heat cycle suggested the formation of Indo-Kollidon[®] VA 64 ASDs across the drug loading range selected in this study.

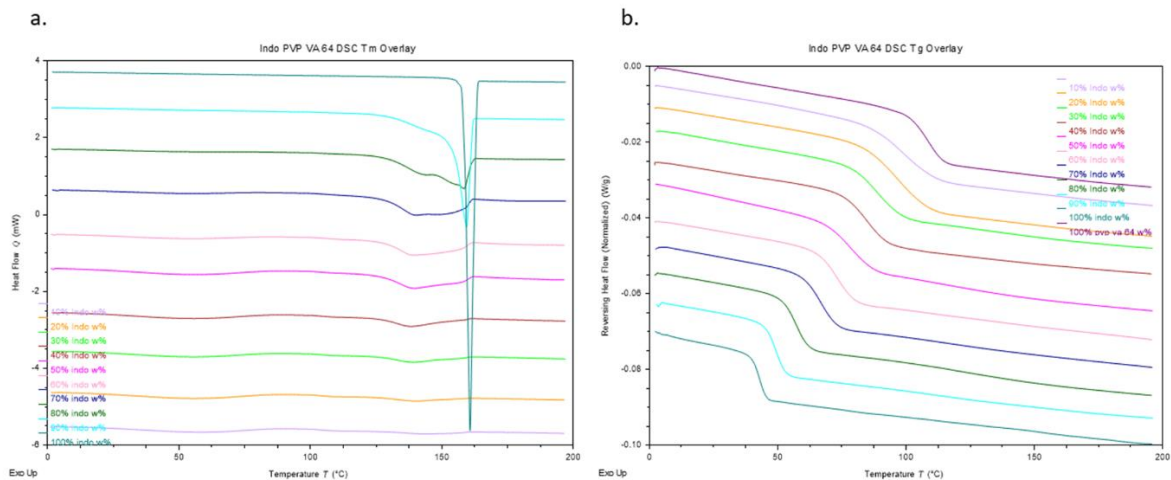


Figure 1.2. Indo-Kollidon[®] VA 64 DSC thermograms overlay. (a) Melting point depression from the 1st heating ramp. (b) ASDs T_g Overlay from the 2nd heating ramp.

Figure 1.3 shows the predicted and experimental T_g for the drug-polymer binary system. Deviations were observed between experimental T_g and calculated T_g by the G-T equation. Positive deviations may lead to stronger interactions between drug and polymer molecules. On the other hand, negative deviations may reflect weak interactions between drug and polymer molecules. In this study, most compositions selected showed positive deviations of the experimental data from the predicted ones. This result suggested strong interactions between Indo and Kollidon[®] VA 64 molecules.

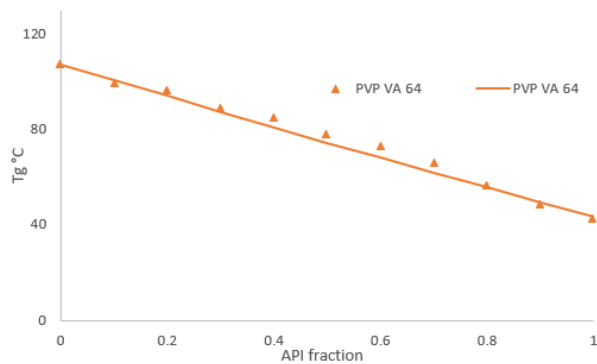


Figure 1.3. Indo- Kollidon[®] VA 64 ASDs T_g of the mixture by DSC (triangle) and G-T equation prediction (solid line).

A plot of $(1/T_{m\text{ mix}} - 1/T_{m\text{ pure}}) \times (\Delta H_{\text{fus}}/-R) - \ln(\phi_{\text{drug}}) - (1-1/m) \phi_{\text{polymer}}$ versus ϕ_{polymer}^2 , as shown in Figure 1.4a, yielded a linear relationship between these two factors. The Indo-Kollidon[®] VA 64 system showed a linear relationship across the drug loading range from 0.70 to 0.90, and the interaction parameter χ value of -6.7382 ($R^2 = 0.9992$) was obtained. This is characterized by the limited melting point depression data observed from the DSC thermal mixing (Figure 1.4). Usually, large positive interaction values were observed for the immiscible drug-polymer binary system through the MPD method. On the other hand, in the current study, the negative χ value suggested Indo and Kollidon[®] VA 64 were miscible within the compositions range [14]. To further understand the drug-polymer miscibility, this study used eq. 4 and the F-H interaction parameter values (χ) to examine the change in Gibb's free energy as a function of drug volume fraction (Figure 1.4b). Gibb's free energy of mixing for this binary system was negative through the composition range 0.10 to 0.90 at room temperature 25 °C and was dependent upon drug volume fraction and temperature.

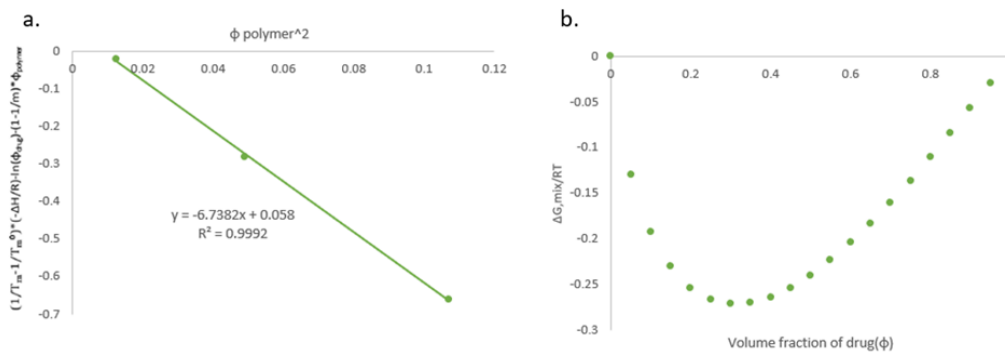


Figure 1.4. (a) F-H interaction parameter plot close to the Indo melting point. (b) Indo-Kollidon[®] VA 64 system $\Delta G_{\text{mix}}/RT$ as a function with drug volume fraction.

Moreover, this study was able to calculate the values for F-H theory A and B constants as manifested in Eqs. 7 where A and B values can be used to calculate interaction parameter χ value at different temperatures, as shown in Figure 1.5 (25, 50, 80, 100, 120, 140 and 160 °C). Therefore, substituting the χ value to Eqs. 4 will give us a broader understanding of Gibb's free energy of mixing as a function of drug volume fraction and temperature. This plot helps map the compositions and temperature for spontaneously mixing. It suggested that Kollidon[®] VA 64 would be miscible with Indo above 100 °C since it showed negative ΔG_{mix} . At 100 °C and above, Indo-Kollidon[®] VA 64 binary system will generate a homogenous mixture and are more thermodynamically stable at all drug loading.

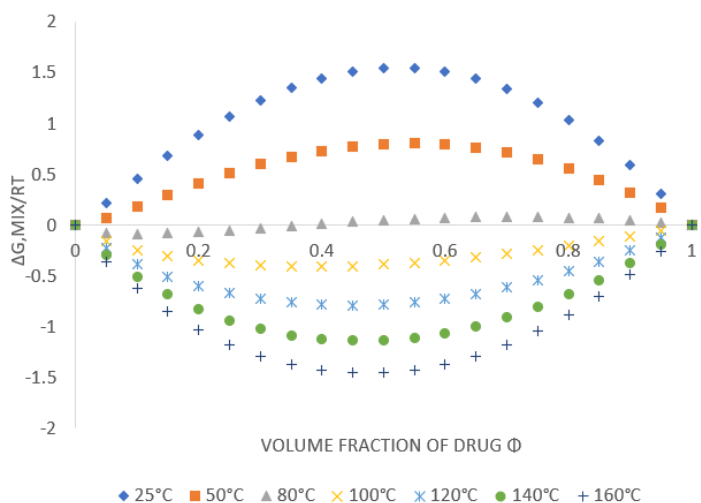


Figure 1.5. Gibb's free energy of mixing/RT as a function of Indo volume fraction for model compound and Kollidon[®] VA 64 system at 25, 50, 80, 100, 120, 140, and 160 °C.

1.3.4. Construction of the Phase Diagram

For Indo- Kollidon[®] VA 64 binary system, this research plotted the ΔG_{mix} as a function of different compositions and temperatures. This information can be combined with T_g to construct

the phase diagram, as shown in Figure 1.6. The glass transition curve was plotted by the experimental data from DSC 2nd heating cycle. Below the T_g curve, the molecular mobility is low, and the phase separation is thermodynamically favored, so it is usually not considered for ASDs development. Most importantly, this phase diagram identifies the drug-polymer binary system phase boundaries. The drug-polymer solubility curve (liquid-solid boundary) was determined by the melting point depression method. Compounds T_m dropped with the addition of the polymer carrier due to the interaction between drug and polymer. Above the drug-polymer solubility curve (zone A and B), considered stable zones, the drug is expected to stay stable in a polymeric carrier, and phase separation is not expected. In general, drugs in this stable range are supersaturated, which can address the drug solubility, dissolution profile, and bioavailability in the gastrointestinal fluids (GI) fluids. Below the drug-polymer solubility curve and above the drug-polymer miscibility curve (zone C and D), which are considered metastable zones. The metastable zone is essential to understanding the supersaturation and phase separation. In zone C and D, it requires activation energy and kinetics effects to overcome the phase separation. At this metastable zone, the compound is metastable supersaturated in the polymeric matrix, which helps prevent the precipitation, and helps to improve the oral dosage absorption. Below the drug-polymer miscibility curve (zone E and F), which are considered unstable zones phase separation is thermodynamically favored, and it is usually not considered for ASD development.

However, ASD formulation crystallization is complex and depends on many thermodynamic factors and storage conditions (e.g., humidity, temperature), and other elements [27]. This research constructed a phase diagram with F-H theory by exploring selected drug-polymer compositions' preferences and thermal stability. It is worth knowing that when the system is under room temperature 25 °C, the ASD formulation would very likely be below the system T_g and is perhaps

kinetically inhibited from recrystallization, which secures long-term stability. Nevertheless, with the phase diagram, we can determine appropriate compositions and processing conditions that lead to a more stable ASDs system, at least from the thermodynamical consideration.

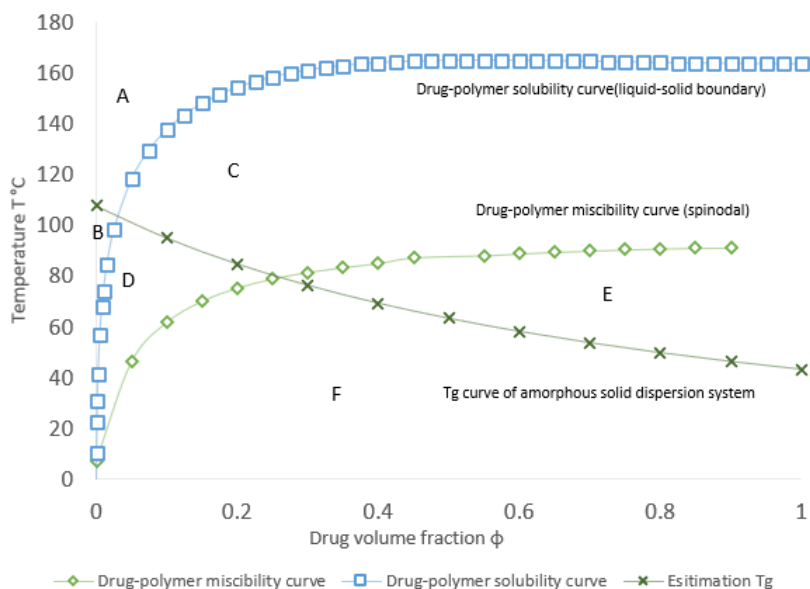


Figure 1.6. Indo- Kollidon® VA 64 binary system phase diagram.

1.3.5 HME Process Design Space

HME technology is one of the most common ways to produce ASD formulations in the pharmaceutical industry. However, it also has limitations, especially for thermal-sensitive drugs and polymers. Usually, if the drug T_m is over 200 °C, it has thermal degradation concerns when the processing temperature is set that high during extrusion. Therefore, it is crucial to map the extrusion temperature range to help us avoid thermal degradation and confirm that the drug is dispersed in the amorphous form in a polymeric carrier. The phase diagram (Figure 1.2a) showed the indomethacin T_m dropped by the addition of the Kollidon® VA 64 under equilibrium conditions,

which allow for the production of Indo dispersed ASD at lower processing temperatures even lower than Indo T_m .

Based on the guidance from the phase diagram (Figure 6), this research identified the stable, metastable, and unstable zone for the Indo- Kollidon[®] VA 64 system. To extend this study, Figure 1.7 clearly illustrates the design space for the HME process, where the drug-polymer solubility curve, indomethacin T_m , and the polymer T_{min} dictate (construct) the design space as shown in the green area. The solubility curve obtained from melting point depression help to select the processing temperature to ensure Indo can fully dissolve in Kollidon[®] VA 64 polymeric carrier. The crystalline drug compound will convert to its amorphous form in these processing conditions by applying sufficient processing time and conditions. Above the HME process design space, the ASD system may be formed, but it has a higher chance of thermal degradation. Under this design space, the operation most likely will not possess sufficient viscosity and temperature for selected drug loading, so it is expected that the drug could not fully dissolve in the polymeric matrix and will form a suspension.

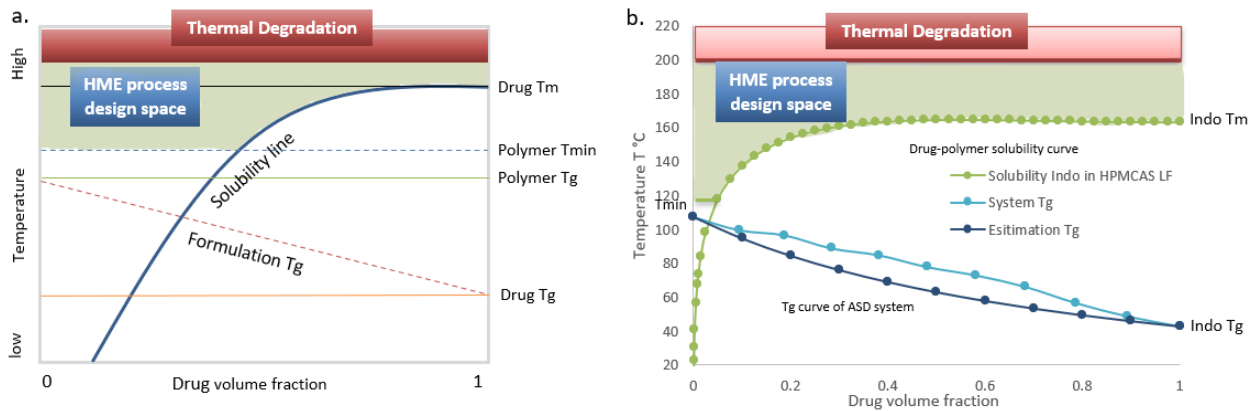


Figure 1.7. The temperature-composition phase diagram for HME process design space application.

1.3.6 Preparation of ASDs by HME: validation of the phase diagram

HME processing parameters were selected based on the information suggested by the temperature-composition phase diagram and the HME design space map. This way could reduce the risk of drug degradation. To investigate the temperature impacts on the extruded ASD formulations, formulations of 20% drug loading were extruded at 120 °C, 150 °C, and 160 °C, whereas for 40% drug loading, the extruding temperature was set at 150 °C, 160 °C, and 170 °C. The HME experiments were executed in triplicate. These process temperatures were selected to represent the stable, metastable, and unstable areas. However, it is difficult to know the physicochemical properties of the filaments based on the phase diagram since the F-H theory did not consider the shearing stress and the mechanical energy input during the extrusion process. Therefore, to further understand each formulation (F1-F6), validation was necessary to the different applied temperatures. The average torque and the physical appearance of the filaments are listed in Table 1 below.

Drug loading (w/w) %	Formulations	Extrusion temperature (°C)	Torque average (Nm)	Filaments physical appearance
20	F1	120	1.87 ± 0.40	Opaque with particles
	F2	150	1.28 ± 0.25	Clear
	F3	160	0.99 ± 0.20	Clear
40	F4	150	1.60 ± 0.25	Clear
	F5	160	1.15 ± 0.36	Clear
	F6	170	0.94 ± 0.23	Clear

Table 1.1. HME processing parameters with physical appearances.

Table 1.1 shows F1-F6 samples processing parameters and the physical appearance changes of the extruded filaments. The average torque value observed decreased with the increasing extrusion temperature with all formulation batches. For 20% drug loading of indomethacin, it showed the lowest torque under 160 °C processing temperature; and for 40% drug loading of Indo, it showed the lowest torque under 170 °C extruding temperature. Since the other process parameters (screw design, screw speed, die size, die temperature) were fixed, the impacts of the barrel temperature on the filament's characterization were clearly observed. The filaments at 120 °C were opaque with surface particles. The torque was the highest; this may be explained by insufficient melting of the drug, which led to the drug particle not being fully dissolved in the polymer carrier. Other formulation batches showed good physical appearance and can be considered for further investigation.

1.3.7 Accelerated stability test by PXRD

The filaments obtained from the HME process were milled into powder and stored under accelerated testing conditions at 40 °C and 75% relative humidity (RH) stability chamber for a month. The stability of ASDs formulations was checked using PXRD at the initial development (Tzero) and after being exposed in the stability chamber for one month. The PXRD results revealed in Figure 1.8 confirmed the amorphization of the Indo in the HME extruded filaments (F2-F6) from Tzero till one month under 40 °C/ 75% RH showed good physical stability of these ASD systems and validated the HME processing setting. F1 formulation (20% Indo) produced under drug-polymer solubility line (120 °C extrusion temperature) showed partial crystallinity at both Tzero and after one month. This is likely because the processing temperature was lower than the

system T_m , so the drug could not totally transfer to the amorphous state. As shown in Figure 8 and Table 2, though F4 filaments produced under drug-polymer solubility line (150 °C) showed drug in the amorphous state retained its form after storage this was likely mediated by strong drug-polymer molecular interactions in addition to the processing temperature (150 °C) close to the binary curve at 40% drug loading. On the other hand, it confirmed that the phase diagram and the HME processing are necessary for optimizing the producing parameters.

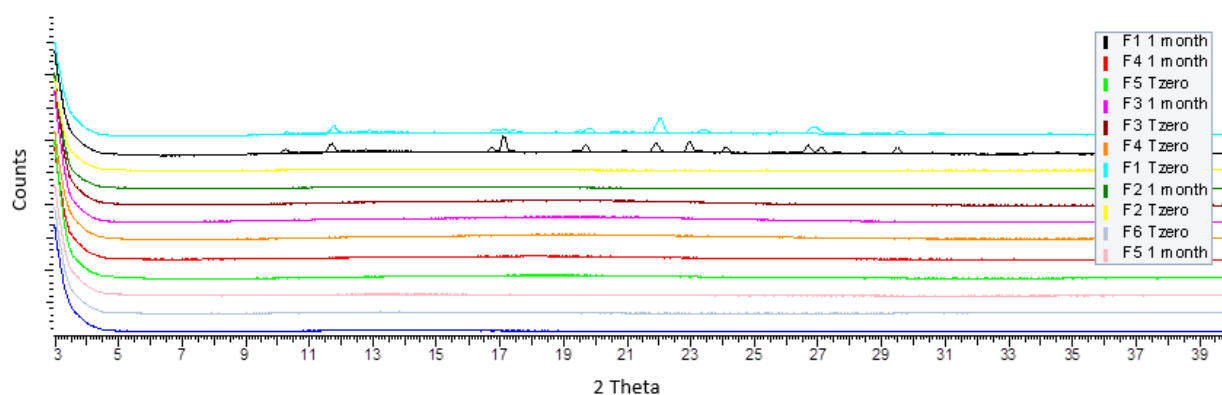


Figure 1.8. XRD overlay for ASDs formulation (F1-F6) at Tzero and 1month under 40 °C/ 75% RH stability chamber.

1.4. Conclusion

This research has proposed a lab-scale method based on the F-H theory to predict the solubility and miscibility of the drug-polymer binary system. Indo and Kollidon[®] VA 64 interaction parameters were obtained by melting point depression and solubility parameter methods. The temperature-composition and Gibb's free energy of mixing phase diagrams above the system T_g were constructed. The phase diagram clarifies the stable, metastable, and unstable zone for the ASDs system. The phase diagram provides a reasonable design space for the HME process of ASDs with the kinetic and thermodynamic considerations allowing for extrusion process at lower temperatures besides inhibiting the recrystallization. This work established fundamental thermodynamic elements for the HME process design as well as the process development.

CHAPTER II

DESIGN OF EXPERIMENT (DOE) IN HOT-MELT EXTRUSION (HME) PROCESS FOR AMORPHOUS SOLID DISPERSIONS (ASDs) FORMULATION OPTIMIZATION

2.1. Introduction

Amorphous solid dispersions (ASDs) have attracted increasing attention due to improving compound solubility, dissolution rate, and oral bioavailability. The drug solubility can be significantly higher once it is dispersed into the polymer carrier compared to its previous crystalline aqueous solubility [32-35]. However, amorphous drugs' Gibbs free energy (ΔG) is higher than the crystalline counterpart. It caused the biggest concern for ASD formulation since it is naturally unstable and easily crystallized. [36,37]. The standard technique to prepare an amorphous solid dispersion formulation includes hot-melt extrusion (HME) (heat-based) and spray drying (solvent-based) [38].

HME was widely used in plastic and rubber manufacturing last century and has now been explored as a strategy for ASDs production in the pharmaceutical industry, which improves the solubility and bioavailability of biopharmaceutical classification system (BCS) Class II and IV drugs with low solubility. HME provides several advantages compared with the solvent-based method for thermally stable materials: eco-friendly, solvent-free, affordable, continuous, and accessible [38]. HME is an application that combines mixing, melting, softening, and conveying simultaneously. The optimization of the HME process in the pharmaceutical area has been considered by formulation development, process parameters, and other factors [38-40].

According to the US Food and Drug Administration (FDA), the highest-quality medicine product is one that consistently and reliably delivers therapeutic performance while also being free of impurities [41]. FDA, European Medicines Agency (EMA), and other international regulatory bodies strongly support the concept of Quality by Design (QbD). QbD was created to ensure a thorough grasp of the pharmaceutical manufacturing process at any stage of the product development cycle, including commercial production. Furthermore, this strategy aimed to promote a more profound knowledge of product and process design and process improvement, scale-up, and optimization [42]. Critical quality characteristics and risk assessment, design space, process analytical technology (PAT), control strategy, and real-time release testing are the primary components of the QbD, as shown in Fig. 2.1 [41-43].

One of the most common techniques used to study QbD is the design of experiment (DoE) [44]. DoE is a designed and systematic approach for establishing a mathematical method to assess the links between input factors influencing one or more output responses. The controlled input factors are methodically varied in the DoE approach to evaluate their impacts on the response variables, allowing for the identification of the most significant input factors, the identification of input factor settings that lead to optimized output responses, and the elaboration of input factor interactions [44,45].

The DoE tests considered screw speed, feeding rate, and barrel temperature as factors. This study analyzed their impacts on the response of drug release rate by exploiting a response surface designs (RSD) model. The central composite design (CCD) analysis is the most commonly utilized RSD experiment in DoE, which identified the influence on the extruded product associated with well-defined factors combination. Using DoE to construct experimentally efficient factors screening and optimizing the response, this study identified critical elements and the optimized

parameter setting that leads to a desirable response. Furthermore, the use of DoE allowed us to gather more information about ASDs formulation solubility. This knowledge will guide the suggestions of polymer and drug compositions to improve decision-making while developing more stable extruded ASDs.

This research investigates the rheological characteristics of a mixture of a model drug and a polymer excipient using rheometers. As a result, the collected rheological data may be utilized to optimize the extrusion process and indirectly estimate the drug's solubility in the polymer excipient, as described in the next section of this paper. In general, if a polymer and a drug form one phase at the processing temperature, the result will be more homogeneous, but it will also have other desired qualities, such as a faster drug dissolution rate [46]. Understanding solubility information may reduce the time spent on trials and comprehend how the drug's physical state varies over the HME preparation and storage period. Despite the apparent advantage and high interest in establishing the drug's solubility in a polymeric excipient, few earlier articles have systematically described how to establish this fundamental data [46,47]. The differential scanning calorimetry (DSC) approach slowly heating a mixed sample from room temperature to the desired temperature such that the kinetics do not impact the solubility results [48]. A longer evaluation time is needed, which may result in the sample's thermal degradation. Researchers will extract the solubility data from the mixture's viscosity at various drug loadings, which only requires a reasonably quick and straightforward viscosity test. Consider a series of API-polymer PM with various drug loadings equilibrated at a temperature lower than the drug's melting point but higher than the polymer's melting/softening point, which is why the drug's solubility in the polymer may be deduced from the mixture's viscosity [49,50]. Because the dissolved small drug molecules improve the mobility of the polymer chain and the free space between polymer molecules, the

mixture's viscosity decreases as the drug loading increases. The mixture comprised crystalline drug particles and a drug-polymer solution above the solubility limit [51].

As a result, this work aims to examine how HME parameter differences affect the physical stability of Indo-based ASDs. Furthermore, rheology studies enable us to select a better composition to stabilize the ASD system from a material science standpoint. This study also focuses on defining a design space for Indo and polyvinyl pyrrolidone vinyl acetate (PVP VA 64) ASD systems using DoE by studying the impacts of processing settings.

Indomethacin (Indo), a BCS Class II (low solubility, high permeability) drug, was chosen as the study's model compound. The polymeric carrier for ASDs was selected as PVP VA 64. This research aimed to prepare ASD formulations of indomethacin with selected polymer and apply essential characterization of the ASDs. Determine the factors contributing to successful ASDs and identify the formulation's compositions. Constructed the temperature-composition phase diagram with F-H theory and then generated an HME process design space diagram to identify the processing condition with the selected composition. Prepared the extruded formulations with the specified temperature range and explained the minimum extenuating temperature based on the thermodynamic considerations.

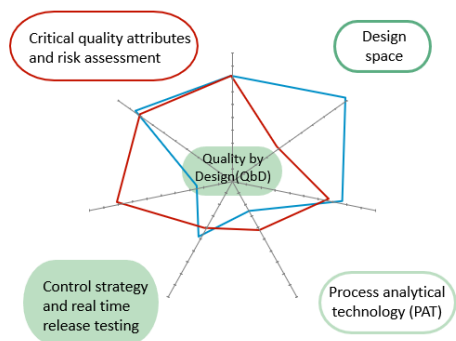


Figure 2.1. Instruction of Quality by design (QbD)

2.2. Materials and Methods

2.2.1. Materials

Indomethacin (purity: >98.0%) was purchased from TCI (Tokyo Chemical Industry Co., Ltd., Tokyo, Japan); Kollidon[®] VA 64 grades of PVP VA 64 was kindly donated by BASF (Florham Park, NJ, USA), and the chemical structure of the indomethacin and Kollidon[®] VA 64 showed in Figure 2.2.

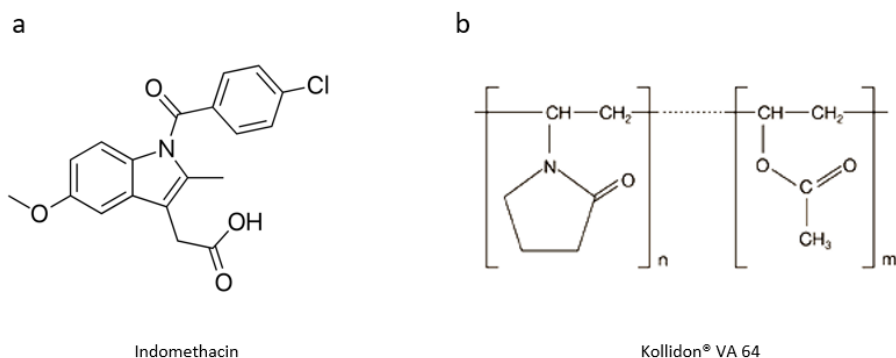


Figure 2.2. Chemical Structure of (a) Indomethacin; (b) Kollidon[®] VA 64.

2.2.2. Physical Mixture (PM) Preparation

To prevent moisture influences, Indo and Kollidon[®] VA 64 were kept in a vacuum oven (Thermo Fisher Scientific, Waltham, MA, USA) for at least two days before further analysis. To obtain a better sample distribution, drug and polymer PM with varying compositions of 10%, 20%, 30%, 40%, and 50% (drug weight fraction w%) were mixed using a MaxiBlend[®] Lab blender (GlobePharma Inc, New Brunswick, NJ, USA) at 30 RPM for 10 minutes (total weight 100.0 g each batch).

2.2.3. Rheology Studies

A rheometer AR 2000 (TA Instruments, New Castle, DE, USA) has been used to determine the dynamically rheological properties of Kollidon[®] VA 64 and its PM with Indo to learn more about the impacts of rheology behavior on the variable composition of Indo-Kollidon[®] VA 64 binary systems. PM (with 10%, 20%, 30%, 40%, and 50% w% Indo loading) were examined further in this research, and 1 g of each sample was pressed into disks of 25 mm in diameter. A sample disk with a diameter of 25 mm and a thickness of 1 mm was placed between two parallel plates for the experiment (25 mm in diameter). At 160 °C temperature constantly, dynamic time sweeps were performed. A 0.05% strain was applied to the sample, with frequencies ranging from 0.1 to 100 rad/s. A dynamic temperature ramp was conducted at a fixed angular frequency of 0.1 rad/s. All samples were heated at a 5 °C/min rate until they achieved 160 °C. All samples' complex viscosity was collected after being put through both experiments. To maintain all the tests within the linear viscoelastic range of substances, a strain of 0.05 % was supplied to all samples.

2.2.4. Design of Experiment (DoE)

Using DoE by JMP, the experimental process and output response were created and studied to optimize the extrusion process parameters (SAS Institute, Cary, NC, USA). A response surface design (RSD) is a collection of sophisticated DoE approaches that provide a whole idea, optimizing the intended response. The central composite design (CCD) is the most popular RSD experiment developed for this subject. The impact of processing parameters during extrusion on the formulation solubility of extruded ASDs is critical to ASD development. Which, in this case, represents the experiment's response: drug release rate at pH 6.8 phosphate buffer.

Furthermore, three different continuous factors were selected barrel temperature (120-160 °C), feeding rate (3-10 g/min), and screw speed (100-400 RPM) to further investigate the impacts of processing conditions on the response.

This study employed the response prediction profiler option based on the response surface design to gain additional information and determine the settings that generate the optimal response target by selecting maximize desirability. The prediction profiler allows to change variables interactively and analyze their impact on the expected response, which isn't possible with experiments. The hot-melt extrusion technology is used for the validation extrusion process as follows. Response surface designs were used to assess the impact of extrusion temperature, feeding rate, and screw speed in a quantitative manner (Table 2.1).

Table 2.1. DoE CCD Design for the experiments.

Formulations	Pattern	Barrel Temperature (°C)	Screw speed (RPM)	Feeding Rate (g/min)
D1	+++	160	400	10
D2	0a0	140	100	6.5
D3	a00	120	250	6.5
D4	---	120	400	10
D5	+++	160	100	10

D6	000	140	250	6.5
D7	+--	160	100	3
D8	000	140	250	6.5
D9	A00	160	250	6.5
D10	00a	140	250	3
D11	0A0	140	400	6.5
D12	++-	160	400	3
D13	---	120	100	3
D14	00A	140	250	10
D15	--+	120	400	3
D16	---+	120	100	10

2.2.5. Preparation of Amorphous Solid Dispersions through Hot Melt Extrusion.

Indo-Kollidon[®] VA 64 filaments were prepared by an 11 mm twin-screw extruder (Thermo Fisher Scientific, Waltham, MA, USA) to discover the effects of barrel temperature and other factors on extruded filament characteristics, followed by DoE response surface design. A twin-screw volumetric feeder (Thermo Fisher Scientific, Waltham, MA, USA) was utilized to feed the PM at different feeding rates (3 to 10 g/min). Formulations were prepared at various barrel temperatures (ranging from 120 to 160 °C) at different screw speeds (100 to 400 RPM). Extrudates were cooled at room temperature. All samples were stored in a desiccator with calcium sulfate and cobalt chloride indicators for further analysis. The standard screw configuration with four

conveying zones and three mixing zones was used for all experiments of 10 g batch sizes of PM. The torque and the filaments' physical appearance were recorded. After cooling to room temperature, the ingredients were ground into fine powders with a mortar and pestle. These optimized extruder parameters were validated by using Indo/Kollidon[®] VA 64 (40:60) (w/w) PM.

The specific mechanical energy (SME) was also calculated to quantify the mechanical energy input during the extrusion process. The SME indicates the amount of power provided by the extruder motor divided by the feed rate of the materials. The calculation of the specific mechanical energy was based on Eqs. (2) and (3), as shown below [52,53]:

$$KW (applied) = KW(motor rating) * \% Torque * \frac{RPM running}{RPM max} * 0.97 \text{ (gearbox efficiency)} \quad (2)$$

$$SME = \frac{KW (applied)}{Feeding rate} \quad (3)$$

2.2.6. Dissolution Studies

Dissolution tests (n=3) were performed on a small lab scale with distilled water to validate the previous drug loading and HME process optimization. Different Indo-Kollidon[®] VA 64 extrudate powders (F1-F5), as shown in Table 2, were weighed (50 mg each) and added to the 20 mL vial with a small stir bar inside when 2ml pH 2 hydrochloric acid (HCl) buffer preheated to 37 °C. After 1 h, added 3x volume (6ml) preheated pH 6.8 phosphate buffer and adjusted the pH. Take 200 uL out at the 1, 2, 3, 4, 5 hours' time points, and samples will be centrifuged for 3 min at 3000 rpm, and the supernatant will be diluted 2x with the mobile phase.

The Indo content was measured using the high-performance liquid chromatography (HPLC) in this section. A Waters Alliance 2695 HPLC (Waters Corporation, Milford, MA, USA) equipped

with a UV detector was used to determine the amount of indomethacin in the extrudate materials (Waters Corporation, Milford, MA, USA). Supelco[®] analytical column (15cm*4.6mm, 3 m column) kept at room temperature (Sigma-Aldrich, St. Louis, MO, USA). The HPLC system was operated at a flow rate of 1 mL/min, with each run injecting a 10 μ L sample and measuring UV absorbance at a wavelength of 235 nm. At HPLC grade, the mobile phase is 50% acetonitrile and 50% water. All chromatographic data were processed and managed using Empower 2 software (Waters, Milford, MA, USA). Indo had a retention time of around 6 minutes. For indomethacin detection, the linear calibration range was 5-200 μ g/mL ($R^2=0.999$).

2.2.7. Analysis of Storage Stability

After cooling down, the extruded filaments generated by the HME process were milled to powder using a mortar and pestle. The storage stability investigation was performed for a month under accelerated testing conditions of 40 °C and 75% relative humidity (RH).

2.2.8. X-Ray Diffraction (XRD) analysis

The amorphous states of extruded powder were examined using PXRD, and the examination was carried out using a D8 Advance Eco diffractometer (Bruker, Billerica, MA, USA). The spectra were obtained from scans performed at 2-Theta (2θ), with a 0.01 ° step size and a 1 s per step period, in the range of 0.0 ° to 40.0 °.

2.3. Results and Discussions

2.3.1. Rheology Studies of Indo-Kollidon® VA 64 System

The powder rheometer has been used to examine the rheological characteristics of the polymer and drug-polymer PM with various ratios (as shown in Fig. 2.3 and 2.4). Fig. 2.3 shows the effect of the Indo concentration on the complex viscosity. At 120 °C, the viscosity decreases with all the PM, and polymer material with the temperature increases. The Indo concentration is up to 40%, indicating the plasticizer effect of the Kollidon® VA 64. In addition, at 140 °C, the viscosity of the 40% w/w Indo-Kollidon® VA 64PM was the lowest compared to other PM and the pure polymer.

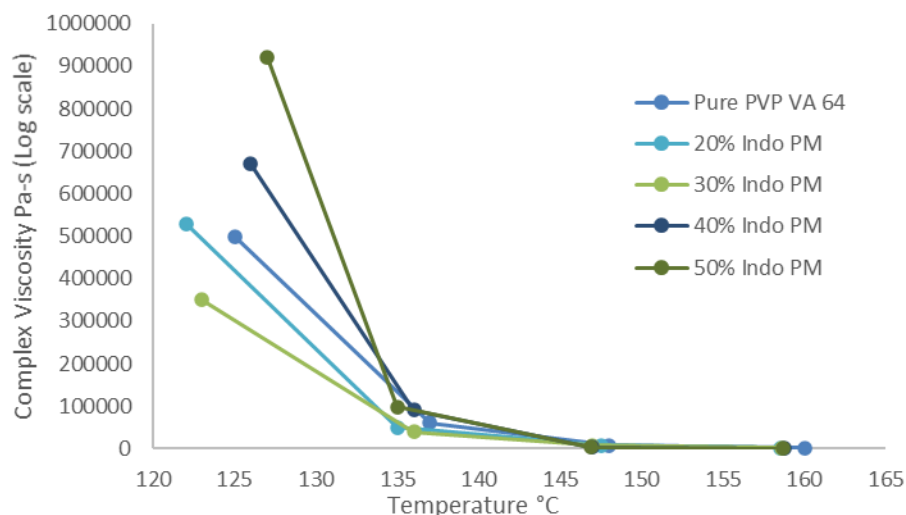


Figure 2.3. The complex viscosity of Indo-Kollidon® VA 64 PM under the temperature ramp at 0.1 rad/s ang. Frequency.

Temperature ramp studies were carried out at temperatures ranging from 120 to 160 °C (as shown in Fig. 2.3). The experiment's results reveal that the complex viscosity of both pure Kollidon® VA 64 and its PM with Indo decreases as the temperature rises. The viscosity of Kollidon® VA 64 and PM was slightly reduced at 135 °C due to the greater shear frequency.

Furthermore, as compared to other PM and the pure polymer, the viscosity of the 40% w/w Indo-Kollidon[®] VA 64 PM at 140 °C was the lowest.

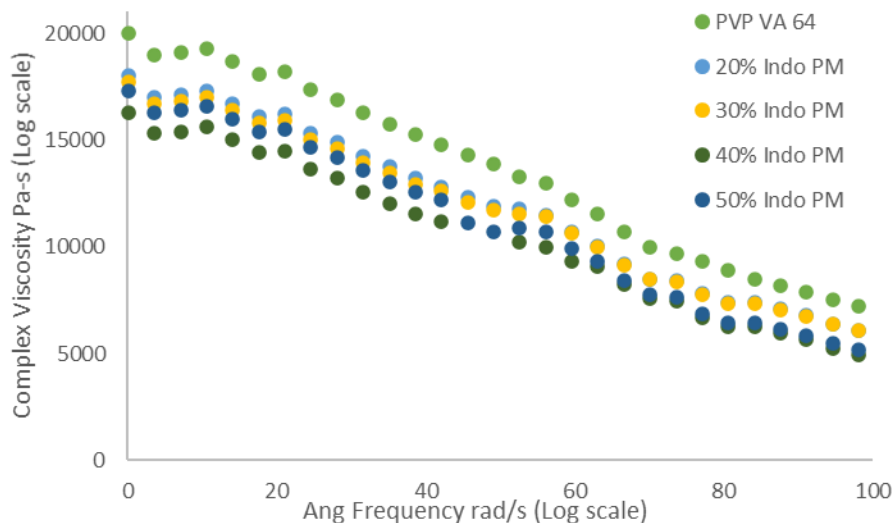


Figure 2.4. The complex viscosity of Indo-Kollidon[®] VA 64 PM under the dynamic frequency sweep at 160 °C temperature.

At the same temperature, Figure 2.3 illustrates that the viscosity variations of Kollidon[®] VA 64 and its PM with Indo stayed within the same trend around the drug melting point under varied shear rates, which is not significant in this case. This can be attributable to Kollidon[®] VA 64's rheological characteristics. The viscosity of the materials and the temperature have an impact on shearing.

The zero-shear viscosity ratio was obtained using the approach previously described to investigate further the miscibility limit of Indo in Kollidon[®] VA 64 [49]. The results are depicted in Fig. 2.7, and more information is provided in Section 3.5. At 140 °C, it was observed that around 40% w/w Indo had the lowest zero shear viscosity ratio, which doses with greater drug loading

mixes. This key point implies that Indo's estimated miscibility limit in Kollidon[®] VA 64 is about 40% drug loading, which has been validated by other approaches [50].

It suggests that a better composition improves PM miscibility. Suppose the dispersed solid particles are single-sized spheres. The reduced viscosity η/η_0 of the PM increases as the volume fraction χ of the dispersed phase increases, as shown by the equation below.

$$\eta/\eta_0 = 1 + 2.5\chi \quad (1)$$

Herein, η is the mixture's viscosity, and η_0 is the viscosity of the pure solvent or molten polymer in our study. Eq 1 suggests that the PM's viscosity will increase with the amount of the drug particles when the solubility limit is passed. The curve's slope depends on factors such as the shape of particles and the potential particle-particle physical interactions. In other words, the slope may vary from 2.5 given here.

The reduced viscosity of Indo-Kollidon[®] VA 64 η/η_0 was determined and presented in Fig. 5 at various concentrations. Each curve was fitted with a polynomial of 5th degree, and a minimum point was found for each curve. As previously stated, the drug's solubility in the polymer is determined by the minimum viscosity point. The viscosity for 50% Indo is higher than that of 40% Indo, indicating that the system had reached the solubility of Indo at that temperature. The decrease in viscosity is very pronounced at lower shear rates up to 10 rad/s and becomes insignificant at high shear rates. The phenomenon suggests that it is better to use a lower shear rate to obtain the drug's solubility data, as shown in Fig 2.5.

In summary, if the viscosity of a drug-polymer PM is plotted against the drug concentration, the slope is expected to be negative below the solubility limit and changes to positive beyond the limit. The critical point on the curve gives the drug's solubility in the polymeric excipient [47]. A

similar phenomenon has been observed in current drug-polymer systems. The viscosity of 50% Indo is greater than that of 40% Indo, suggesting that perhaps the system had attained solubility at the temperature. As shown in Fig 2.5, choosing the 40% drug loading is preferable to investigate more.

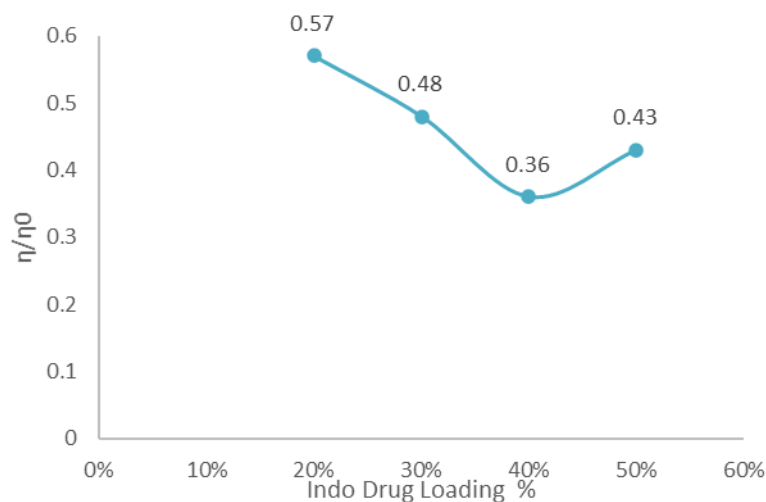


Figure 2.5. The predicted miscibility limitation of the Indo-Kollidon[®] VA 64 PM at 160 °C by zero shear viscosity method.

2.3.2. Hot melt extrusion parameters optimization by DoE

The extrusion temperature was the research's first variable. In an attempt to develop an amorphous solid dispersion system, HME requires thermal energy to melt the particles. The melting point, thermal stability, glass transition, and desired formulation all play a role in determining the best barrel/ processing temperature. Heating components situated within the extruder barrel were used to maintain the extrusion temperature. The extrusion employed in this investigation may reach 200 °C. Because of the vast temperature range, it was necessary to narrow down this parameter and limit the number of experiments. In the current investigation, the

formulations were prepared underneath this temperature, which avoided the minor thermal instabilities risk, reducing the first high temperature from 180 °C to only 159.83 °C in Fig 2.6.

The screw speed was the study's second variable. The resident time, shearing force, and extrusion torque are all affected by screw speed. Low screw speed allows for more heat and less shearing force in the formulation and vice versa. To modify the screw speed, examine the parameters of the formulation, such as viscosity, melting point, and stability. High-viscous materials, for example, will necessitate a slow processing screw speed. Due to extruder torque and pressure, screw speed may be restricted. According to preliminary research, while using a high screw speed, the molten Indo-Kollidon[®] VA 64 matrix demonstrates a high torque value. On the other hand, the extrudates became irregularly informed when the screw speed remained low. This one was attributed to decreased backpressure, a key element in extrudate sculpting [51]. From Fig 2.6, the optimized screw speed in this research is 256.60 RPM.

The feeding rate is the final parameter being discussed in this examination. The feeding rate impacted the particle size, screw speed, and extrusion temperatures were all affected by the feeding rate. As shown in Figure 6 below, the optimized feeding rate by DoE is 7.35.

Identifying the optimal conditions for the intended objective is the most critical part of response surface design. To find the significant parameters, a screening or factorial experiment was employed first (temperature, pressure, cooling rate). A response surface-designed study can be used to select the optimal parameters for each variable. Fig 2.6. shows the result of the most desirable settings to meet the response. Furthermore, as previously stated, the optimized extruding parameters are not an actual experiment setup, but rather new parameters based on the experimental data, which will be validated in subsequent experiments.

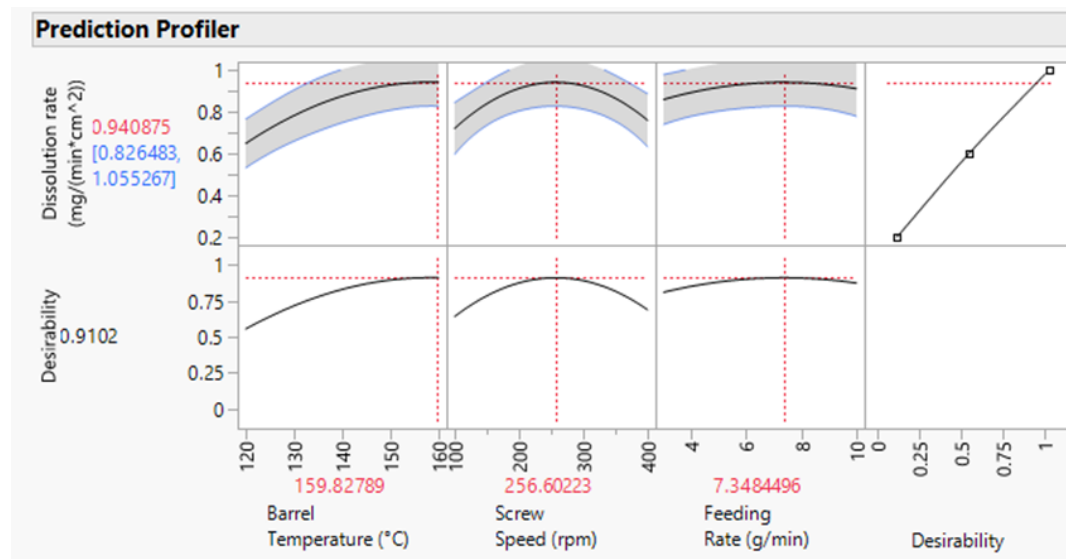


Figure 2.6. Prediction profiler for the DoE Response Surface Analysis.

2.3.3. Hot-melt Extrusion and Preparation of Indo-Kollidon® VA 64 ASDs: Validation for DoE optimization.

Four HME runs were conducted using five different formulation designs (F1-F5), which consisted of different drug loading and the optimized extruding parameters above, as shown in Table. 2.2. Each run was composed of multiple batches by varying the barrel temperature and screw speed to study the influence of these parameters on SME (as shown in Table 2) and the preparation of Indo-based ASDs.

Table 2.2. HME processing parameters and physical-chemical characterizations of optimization design.

Formulations	Indo	Kollidon®	Torque	Barrel	Screw	Feeding	SME	Indo
	o	VA 64	(N*m)	Temperature	w	rate	kWh/kg	ASDs
		(% w/w)		e	speed	(g/min)		

	(% w/ w)		°C	(rpm)			(yes/n o)	
F1	100	0	9.55±0.1	159	256	7	1.763	No
			4					
F2	20	80	4.71±0.0	159	256	7	0.419	Yes
			9					
F3	30	70	4.74±0.3	159	256	7	0.436	Yes
			5					
F4	40	60	3.93±0.2	159	256	7	0.385	Yes
			7					
F5	50	50	5.59±0.1	159	256	7	0.682	Yes
			6					

Table 2.2 shows the F1-F5 samples' processing parameters and the extruded materials' physical-chemical characterizations of optimization design changes. The average torque value observed decreased with the polymer in all batches. It showed the lowest torque under 40% Indo loading in this study. Since the other process parameters (screw design, die size, and die temperature) were fixed here, it's clear to illustrate the function of the optimized extrusion parameters and the validation of the PM rheology studies. It suggested sufficient melting of the drug at the current temperature and speed, which leads to the drug particle being fully dissolved in

the polymer carrier. Other formulation batches showed good physical-chemical properties too in this study and can be considered for further investigation.

As the previous section described, all batches' formulations used the same standard screw configuration, so SME was not controlled by screw design in this case. Thus, other extrusion parameters were studied. As shown in Table 2.2, by increasing the Indo content from 20% to 50% at 160 °C, the SME was increased from 0.419 to 0.682 kWh/kg. This influence of the drug content (F2-F5) on the SME was also observed at 160 °C when compared with the raw polymer F1 (1.763 kWh/kg).

Moreover, adjustments in the drug loading had effects on SMEs, showing the lowest SME (0.385 kWh/kg) at 40% Indo loading. From Table 2.2, it is clear that the SME decreased as the drug loading increased to 40% drug loading. At 50% drug loading, SME changed the direction and went higher. It is probably caused by the drug-polymer interaction, consistent with the PM rheological anticipation from Fig 5 (40% Indo loading is the miscibility limit for this ASD system). It is worth knowing that the extruder's screw speed, feeding rate, and barrel temperature are optimized here by DoE, so they did not show impacts on SME, but it is worth further investigation in the future for this part.

However, the amount of polymer loading did significantly influence torque value. Increasing the polymer composition decreased the torque compared with the pure Indo average torque of 9.55 ± 0.14 N·m. Moreover, the lowest torque value was shown at 40% Indo loading, which indicates this drug-polymer system is the easiest one to operate, confirming the PM rheological expectation.

2.3.4 Dissolution studies

Fig. 2.7 depicts the dissolution profiles of all Indo-Kollidon[®] VA 64 extrudates powder (F2-F5) at pH 2 HCl buffer and pH 6.8 phosphate buffer, as well as the pure crystalline Indo powder F1 dissolution behavior. Starting with the pH 2 HCl buffer studies, it is clear to see that the drug release % of indomethacin at 40% drug (F4) loading has the fastest drug release at both low and high pH, which validates the previous observation of the extrusion process torque and SME, as well as the PM rheological miscibility limit assumption. Moreover, all compositions of extruded ASD powder showed a better release profile than the crystalline Indo in 6 hours, which confirmed the ASDs formulation could significantly improve the dissolution rate over its crystalline form. Though ASD systems always have the concern of being unstable, it is crucial to monitor the physical and chemical stability of the products.

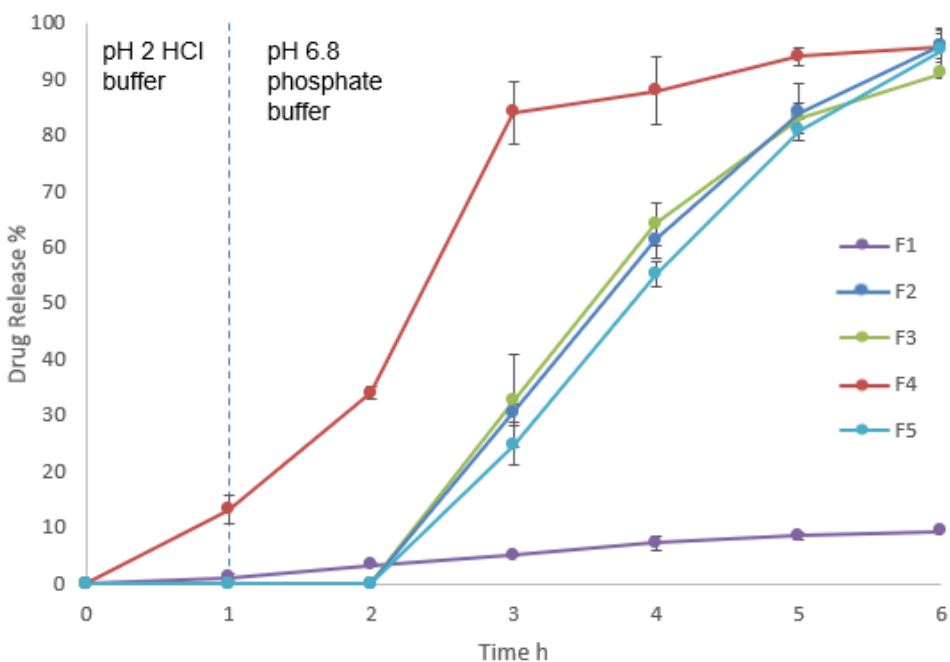


Figure 2.7. Dissolution profiles of indomethacin released from the extrudates powder and of the pure Indo.

The effect of the dissolving medium pH and drug loading on the dissolution performance of indomethacin-Kollidon[®] VA 64 extrudates was investigated in the present research. The experiments were carried out at pH 2 to replicate mimic environments and pH 6.8 to mimic post-stomach environments. This research discovered that indomethacin has a low detectable dissolving rate at pH 2. Still, a higher rate at pH 6.8 indicates the drug release mechanism is dependent on the highly water-soluble Kollidon[®] VA 64. The poor dissolving performance at pH 2 for the other drug loadings (20 % or higher) is due to the production of an amorphous and hydrophobic coating of the drug, which prevents drug release from the compact's interior. The change in pH from low to above the indomethacin pKa of 4.5 dissolves the coating and allows the extrudates to dissolve. We believe that the suggested pH-dependent dissolution model may also be used to control and modulate drug release in the stomach and small intestine for a broad range of poorly soluble ionizable drugs in the future.

2.3.5. Accelerated stability test of Indo- Kollidon[®] VA 64 ASDs by PXRD

The pre-milled filament powder obtained from the HME process was held under accelerated testing conditions at 40 °C and a 75% relative humidity (RH) stability chamber for a month. PXRD tested the stability of ASD formulations after one month of exposure in the stability chamber. The PXRD data in Figure 2.8 confirmed the amorphization of HME extruded F2-F6 powder after one month at 40 °C and 75% RH also the PM and pure Indo (F1), demonstrating the ASD systems' strong physical stability and validating the HME processing setup. The F1 formulation (20% Indo) developed under the drug-polymer solubility line (120 °C extrusion temperature) exhibited partial crystallinity at one month. This is more than likely owing to the processing temperature is lower than the system T_m , preventing the drug from fully transferring to the amorphous form in this situation. Even though F4 filaments were formed at temperatures lower than the drug-polymer

solubility limit (150 °C), XRD data revealed that F4 remained in amorphous forms of the drug. Strong drug-polymer molecular interactions are most likely to blame. Strong drug-polymer molecular interactions are most likely to blame. Furthermore, at 40% drug loading, the processing temperature (160 °C) is near the binary curve. It did, however, demonstrate that the phase diagram and HME processing are required to improve the manufacturing parameters.

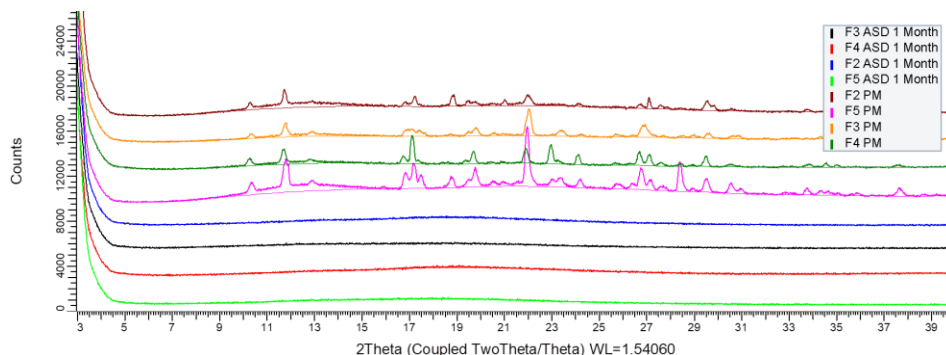


Figure 2.8. XRD overlay for ASDs formulation (F1-F5) PM and after one month under 40 °C/ 75% RH stability chamber.

After accelerated storage, the fore samples (F2-F5) still didn't show percentages of crystallinity, as indicated in Figure 8. As we know, the crystallinity of Indo ASDs can be affected by both SME and torques. Nonetheless, at a 160 °C processing temperature, the effect of SME on the stability of Indo ASDs was negligible in this research. Samples F2-F5 were all treated at the same barrel temperature but with different SMEs, and they didn't crystallize similarly after one month of accelerated conditions. These observations may also be limited by the XRD detectable limitation, which is that if the crystalline percentage is under 5%, there is a high chance it will not be detectable.

2.4. Conclusions

This research has proposed the influence of various processing parameters of HME on the pharmaceutical performance of the Indo solid dispersion system, using a 3-level full factorial statistical design. The results showed that processing parameters have a significant influence on the pharmaceutical properties of Indo solid dispersion. Screw speed, feeding rate, and barrel temperature were found to be affecting processing parameters on the pharmaceutical performance of Indo extrudates properties. The unique and straightforward functional CCD designs by DoE allow the evaluation of each factor and, therefore, the production of the optimized formulation. The DoE concept reduces the cost and time required while providing a high percentage of success by obtaining the most information in the fewest number of experiment runs. This method will reduce the number of experimental trials while obtaining good final-product quality.

From the discussion above, key findings emerge: this research investigates mechanical and thermal energy influences on the preparation and physical stability of Indo-Kollidon[®] VA 64 ASDs. We demonstrate that extruders generate thermal energy that is more effective in the amorphization of Indo in Kollidon[®] VA 64. We also show that small extruders exhibit thermal energy input that has more impact on achieving a homogeneous ASD system, which results in better physical stability. Finally, based on QbD, this study defined a DoE drive optimized processing parameters setting for Indo-Kollidon[®] VA 64 by understanding the difference in effects on dissolution behavior. Extensive results carried out show that this method improves the workflow of ASDs formulation production by HME technology and provides insight into the relationship between mechanical and thermal energies and the preparation and physical stability of Indo-based ASDs.

CHAPTER III

DEVELOPMENT OF CONTROLLED RELEASE ORAL DOSAGES BY DENSITY GRADIENT MODIFICATION VIA THREE-DIMENSIONAL (3D) PRINTING AND HOT-MELT EXTRUSION (HME) TECHNOLOGY

3.1. Introduction

Extensive research has been conducted on HME applications in the pharmaceutical industry for years due to its versatile usage and economic benefits. HME technology is known for its ability to support the development of different dosage forms, especially benefiting poorly water-soluble active pharmaceutical ingredients (APIs) to produce ASD formulations. The research revealed that ASD has significantly improved the dissolution rate, solubility, wettability, and oral bioavailability of APIs and masks the bitter taste of an API [54-57]. HME is a continuous process that extrudes filaments by heating the API and excipients to a specific temperature and pushing them through a shaped die. The resulting filament's quality is affected by the design of the mixing zone, the feeding rate, the screw configuration, the barrel temperatures, and various other factors. In addition, HME helps to change the drug release profile to formulate both immediate release and controlled release dosages as needed [54-57].

During the HME process, a homogeneous mixture of drugs and excipients is rapidly heated and mixed in the equipment, and then the material is pressurized through the extruder into filaments [54,55]. In recent years, researchers have taken filaments created through HME and used them in 3D printing to create many things. Their achievements have also proved that this novel

technology has excellent potential for developing pharmaceutical products [58]. Zhang and colleagues (2016) have used acetaminophen and hydroxypropyl methylcellulose (HPMC) based polymers to develop a controlled release formulation by coupling HME and 3D printing technologies. Furthermore, this study observed the impact of the infill density on the tablet's performance [59].

3D printing is revolutionizing the pharmaceutical industry by promoting personalized therapy, and it has many advantages over traditional dosage forms. For example, it can easily modify the shape, dosage, size, and density to meet the different needs [59-61]. Furthermore, FDM 3D printing technology has been broadly used to produce immediate release drug delivery systems [62] and controlled release [63] drug delivery systems. The Food and Drug Administration (FDA) approved the first 3D printed prescription drug called Spritam® (Aprecia Pharmaceuticals, Langhorne, PA, USA) in 2015 to treat partial epileptic seizures. It has been successfully marketed in the USA. This new dosage form (fast-melt tablets) requires little water to allow the tablet to dissolve quickly in the mouth, which is helpful for people who have difficulty swallowing [60].

However, there are a variety of 3D printing technologies available in the market for producing pharmaceutical dosages, which include selective laser sintering (SLS), fused deposition modeling (FDM), and stereolithographic (SLA) based approaches [59]. The FDM 3D printer is one of the most popular because of its advantages, such as low price and ease of operation. The process started with a 3D digital object created by a computer-aided design (CAD) program and saved as digital stereolithography (.stl) file. FDM 3D printers use a melted filament to build the object through layer-by-layer printing [61,64]. The next layer cannot start printing until the last layer is wholly printed and cured. This curing process is repeated until the object is finished [63,64]. The most common 3D printing material of the FDM 3D printer is polylactic acid (PLA). PLA is a

ubiquitous synthetic plastic with a low melting point and can be easily printed at 180 °C. In this investigation, PLA also was employed as a reference to evaluate and compare the extruded filaments to fit 3D printing requirements, such as hardness, toughness, and stiffness [65]. The texture analysis (TA) evaluated these characters of filaments in this article.

In this study, ketoprofen was chosen as the model drug. Ketoprofen is a weak acid drug- assigned to biopharmaceutics classification system (BCS) Class II, with low aqueous solubility and high permeability. HPMC-based polymers were used as the polymer matrix, and they are also one of the most common polymers used for ASDs manufacturing by HME technology [66]. These drug-polymer-loaded filaments, which were prepared by HME, were then used to make the uniquely designed 3D printed tablets with different infill densities. The tablets were evaluated using kinetic models through their in vitro drug release performance. This research demonstrated the relationship between the infill density of the 3D printed tablets with the in vitro release kinetics.

In summary, this study applied an innovative design of a 3D printed tablet structure, which was combined with a loose shell and compact tablet core, to demonstrate how a printed tablet's density affected the speed of a drug's release. Furthermore, this paper investigates how simply changing the different density gradient settings during printing can allow the formulation to have a controlled release profile without modifying the formulation compositions. Subsequently, mathematical dissolution models were used to elicit further data and received a comprehensive understanding of the 3D printed ketoprofen core-shell structure tablets in vitro behavior.

3.2. Material and Methods

3.2.1. Materials

Ketoprofen is a model API procured from LGM Pharma (Jersey City, NJ, USA). Benecel™ hydroxypropyl methylcellulose (HPMC) K4M, AquaSolve™ hydroxypropyl methylcellulose acetate succinate (HPMCAS) HG, and Klucel™ hydroxypropyl cellulose (HPC) LF, were kindly donated by Ashland (Wilmington, DE, USA). Other analytical-grade chemicals used in the study were obtained from Fisher Scientific (Hampton, NH, USA).

3.2.2. Formulations

The filaments used in the tablet’s core (F1) were made with 30% (w/w) ketoprofen, 50% (w/w) HPMC K4M and 20% (w/w) HPMCAS HG; the filament used in the tablet’s shell (F2) was made with 30% (w/w) ketoprofen, 50% (w/w) HPMC K4M and 10% (w/w) HPMCAS HG 10% HPC LF. Two formulations were listed in Table 3.1.

Table 3.1. Formulation composition for extrusion.

Formulations	Ketoprofen	HPMC-K4M	HPMCAS	HG	HPC LF
	w/w%	w/w%	w/w%		w/w%
F1	30	50	20		0
F2	30	50	10		10

3.2.3. Hot melt extrusion (HME) Process

Physical mixtures (PM) of 100g of both F1 and F2 were prepared separately and mixed using a MaxiBlend™ blender (GlobePharma Inc, New Brunswick, NJ, USA), which was run at 30 RPM for 30 min to ensure an even distribution of samples before the HME process. A Thermo Scientific process 11 parallel twin-screw extruder (Thermo Fisher, Waltham, MA, US) was used to prepare 10g batch sizes for both F1 and F2’s formulations. Then, the premixed formulations were extruded employing the standard screw configuration (Figure. 3.1) at 150 °C with a screw

speed of 50 RPM in all zones. As per the requirement of filament diameter (1.7 mm) of the FDM 3D printer, a 1.5 mm rounded shape die was chosen to extrude filaments.

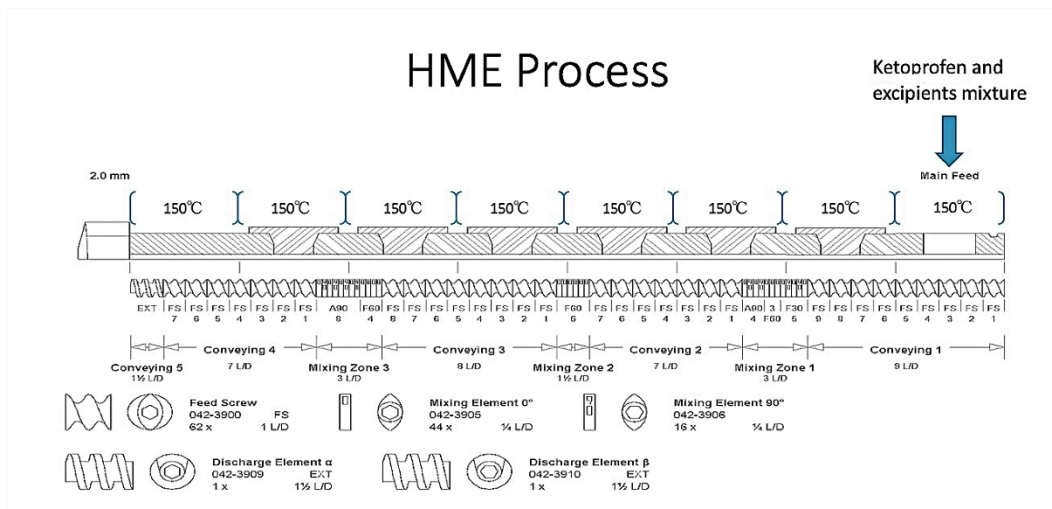


Figure 3.1. Standard screw configuration of Thermo Scientific™ Pharma 11 Twin-screw Extruder.

3.2.4. Filaments Texture Analysis (TA)

A stiffness test was performed using the TA-XT2i analyzer (Texture Technologies, Hamilton, MA, USA) to optimize the formulations and filaments better, as shown in Figure 3.2. Smooth and even extruded filaments were selected for texture analysis, and each segment was cut 5 cm long. For all formulations, the stiffness test speed was set to 2 mm/s, and the trigger force was set to 5.0 g. Ten filaments for each formulation were tested; data collection and analysis were performed using Exponent software version 6.1.5.0 (Stable Micro Systems, Godalming, UK). The stiffness is the key to determining the filaments to be successfully printed. The stiffness is obtained using the following formula:

$$\text{Stiffness} = \frac{F}{\delta} \quad (1)$$

The applied force is F , and deformation is δ in this equation. Each group of filaments was tested and printed ten times, and the filaments that were successfully printed more than six times are considered adequate for 3D printing.

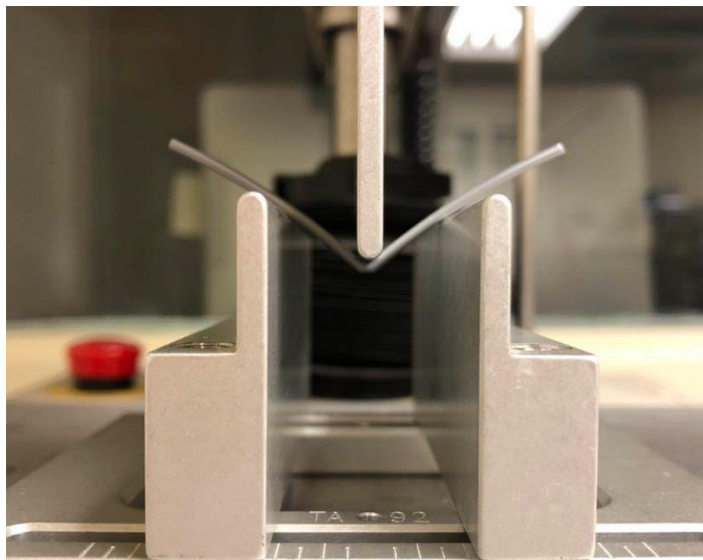


Figure 3.2. PLA texture analysis test.

3.2.5. Differential Scanning Calorimetry (DSC)

The physical blend, the filaments, and the printed tablets were analyzed using DSC to measure the thermal characteristics. The TA DSC 25 (TA Instruments, New Castle, DE, USA) was utilized to measure and analyze around 5 mg samples each time. Samples were packed inside a Tzero aluminum pan (TA Instruments, New Castle, DE, USA) covered with an aluminum hermetic lid (TA Instruments, New Castle, DE, USA). Then, heat the sample and an empty reference pan with a heating rate of 25 °C / min from 25 °C to 200 °C. Ultra-purified nitrogen was applied as the purge gas at a 50 mL/min rate. Results were collected and analyzed by Trios software (TA Instruments, New Castle, DE, USA).

3.2.6. 3D Printing

Autodesk® Fusion 360™ (Autodesk, San Rafael, CA, USA) was utilized to design the tablet model in this study. The selected dosage form's geometry was a tablet consisting of a cylindrical shell with a core inside, as shown in Figure 3.3. It was then exported as a .stl file to be used with an Original Prusa i3 MK3S kit (Prusa Research, Prague, Czech Republic) FDM 3D printer. The HME process prepared the extruded filaments before being pushed through the FDM printer's nozzle above the drug melting point to print the desired dosage form.

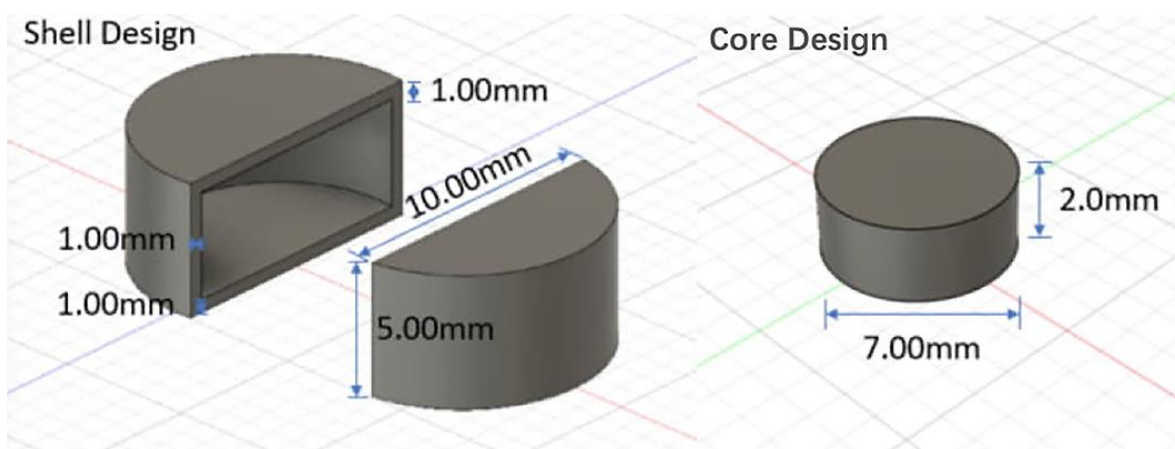
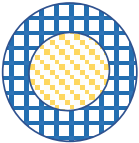
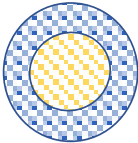
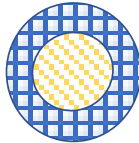
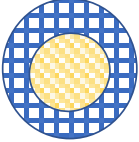
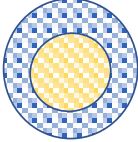
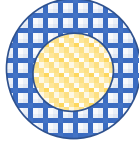
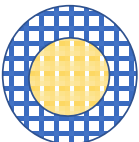
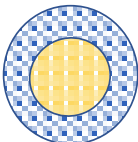
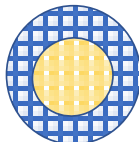


Figure 3.3. 3D printing design.

To ensure the printing process, the control operations of 3D printing were completed through Ultimaker CURA software version 3.4.1 (Ultimaker, Geldermalsen, Netherlands). The printing temperature and the build plate temperature were set at 200°C and 45°C, respectively, and the printing speed was kept at 60 mm/s, layer height was set at 0.1 mm. The core and shell combination density of all nine formulations in Table 3.2, were set differently. The core density was set higher as 40%, 50%, 60% infill, respectively; the shell was designed more porous and looser with a lower density as 20%, 30%, 40%, respectively. The rest of the settings were kept the same.

Table 3.2. Density gradient modification 3D Printing tablets design.

Core Density \ Shell Density	20%	30%	40%
40%	T1 	T2 	T3 
50%	T4 	T5 	T6 
60%	T7 	T8 	T9 

3.2.7. X-Ray Diffraction (XRD) Analysis

The amorphous states of extruded filament were examined using powder XRD, and the examination was carried out using a D8 Advance Eco diffractometer (Bruker, Billerica, MA, USA). The spectra were obtained from scans performed at 2-Theta (2θ), with a 0.01° step size and a 1 s per step period, in the range of 0.0° to 40.0° .

3.2.8. Scanning Electron Microscopy (SEM)

The cross-sections and surfaces of the printed tablets shell and core were analyzed using a JSM-7200 FLV field-emission scanning electron microscope (SEM) (JEOL, Peabody, MA, US). A gold layer covers all samples by a gold sputtering system for 30 s at 70 mTorr pressure for visualization. The picture was taken by a hybrid objective lens, the new combination of magnetic lens and electrostatic lens.

3.2.9. Tablets Physical Parameters

VWR[®] Digital Calipers (VWR[®], Radnor, PA, USA) were used to check every tablet's diameter and height. Forty-five tablets from nine formulations (T1-T9) were tested here, and each tablet was measured five times at different locations. The standard tablet hardness tester VK200 (Agilent Technologies, Santa Clara, CA, USA) was applied to determine the hardness of the tablets; each formulation was tested five times.

3.2.10. In Vitro Drug Release Study

Following the tablet morphology test, each formulation (T1-T9) was quantitatively analyzed for the ketoprofen release profile using The Hanson SR8-Plus[™] Dissolution Test Station (Hansen Research, Chatsworth, CA, USA) employing United States Pharmacopoeia (USP)-II Dissolution Apparatus. 3D printed tablets of each grade were exposed to 900 mL phosphate buffer (pH 6.8) for 24 hours in a 1000 mL standard dissolution vessel. The dissolution system was maintained at 37 °C ± 0.5 with the 50 RPM paddle speed. Samples were collected at 0.25, 0.5, 0.75, 1, 2, 4, 6, 8, 12, 24 hours. The dissolution test followed the same protocol for all 3D printed tablets and was conducted in triplicate (n=3). The amount of ketoprofen was detected by Waters alliance model 2695 high-performance liquid chromatographic (HPLC) Waters Corporation, Milford, MA, USA) equipped with a Supelco[™] analytical column (Col: 176607-04; BL: 9277, 15cm*4.6mm, 3µm) maintained under room temperature. The UV absorbance was measured at 246nm wavelength. The mobile phase was prepared using HPLC grade water for the aqueous phase and HPLC grade methanol for the organic phase at a 30:70 ratio. The flow rate was set at 1 mL/min, and injected 10 µL sample each run. The sample analysis was performed using Empower 2 software (Waters Corporation, Milford, MA, USA). The estimation of ketoprofen was performed using a calibration curve ranging from 1-94 µg/mL ($R^2= 0.999$).

3.2.11. Dissolution Mathematical Model Study

OriginPro 2018 64bit (OriginLab, Northampton, MA, USA) was used to analyze and create the dissolution curve in this study. The non-linear fitting was applied to the previous in vitro drug release test data to draw and analyze its relative curve. The standard mathematical release models of dissolution (zero-order kinetic release model, first-order kinetic release model, Higuchi model, Ritger-Peppas model, and Peppas-Sahlin model) were applied to fit the dissolution data. This study's correlation coefficient (R^2) was an essential parameter to judge its degree of fit [67].

In order to create a reliable mathematical dissolution model, the evaluation of the different models was studied to predict the dissolution curve of the 3D-printed drugs. When a particular mathematical function expresses a specific dosage's dissolution rate, it is easier to make a quantitative analysis of the dissolution prediction. In this case, a total of five major release kinetic models were studied: zero-order, first-order, Higuchi, Ritger-Peppas, and Peppas-Sahlin models [67, 68].

Zero-order Kinetic Release Model

The equation here can be described as:

$$Q_{(t)} = Q_0 + K_0 t \quad (2)$$

Where $Q_{(t)}$ is the release amount of the drug at time t , K_0 is the zero-order constant. It represents a zero-order dissolution rate, and Q_0 is the initial amount of the drug in the solution at the initial state (generally, when $t=0$) [69].

First-order Kinetic Release Model

This model can be described as:

$$\ln Q_{(t)} = \ln Q_0 + K_1 t \quad (3)$$

Where $Q_{(t)}$ is the release amount of the drug at time t , K_1 is the first-order dissolution rate. In this circumstance, the percentage of drugs eliminated per unit time in the body remains constant [70].

Higuchi Model

The Higuchi model first described the drug release rate from the matrix system form published in 1961. The $Q_{(t)}$ is given as:

$$Q_{(t)} = Q_0 + K_H\sqrt{t} \quad (4)$$

Where $Q_{(t)}$ is the release amount of the drug at time t , K_H is the Higuchi model's drug release rate, and this model is the most common model to describe the drug release for the controlled release formulations [71, 72].

Ritger-Peppas Model

The Ritger-Peppas model describes the drug release from a polymeric system when the release mechanism is unclear. The Ritger-Peppas model follows the formula:

$$\frac{Q_{(t)}}{Q_{(\infty)}} = kt^n \quad (5)$$

Where $Q_{(t)}$ is the release amount of the drug at time t , $Q_{(\infty)}$ is the release amount of drug at the time ∞ , k , and n are coefficients [73].

Peppas-Sahlin Model

The Peppas-Sahlin model is the correction formula of the Ritger-Peppas formula. This function can calculate both diffusional and relaxational mechanisms during drug release from a polymeric system developed by Peppas and Sahlin in 1989 written as:

$$\frac{Q(t)}{Q(\infty)} = K_1 t^n + K_2 t^{2n} \quad (6)$$

$Q(t)$ is the release amount of the drug at time t , Q is the release amount of the drug at the time ∞ , k_1 , k_2 , and n are constants [74].

3.3. Results and Discussion

3.3.1. Thermal Analysis

To verify the formation of ASDs, DSC data was gathered for both the homogeneous powder mixtures and the 3D printed tablets. Core, shell, core printed, and shell printed curves in Figure 3.4 represented the curves for homogeneous F1, F2 mixtures powder and the core, shell product after HME and 3D printing process. The original formulation blends DSC curve peaked at about 93 °C. It can be seen that after the HME and 3D printing process, there were no peaks in F1 and F2, which shows that ketoprofen successfully formed amorphous solid dispersion and achieved the amorphous state with the polymers.

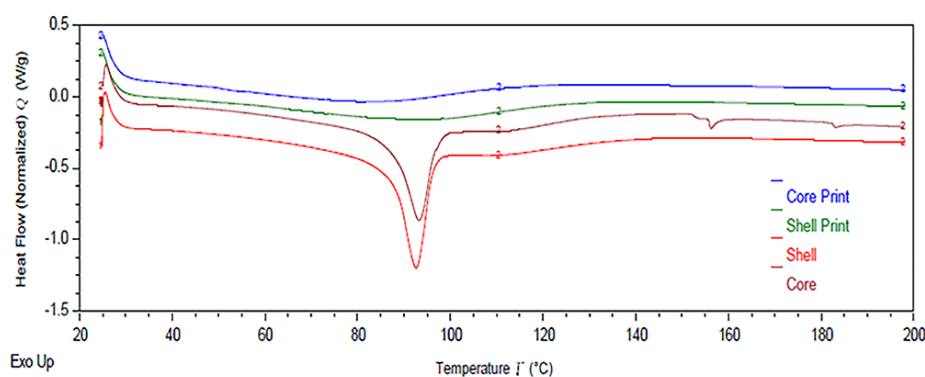


Figure 3.4. DSC thermogram for F1 (Core) and F2 (Shell) homogeneous mixture and the printed core and shell ground powder.

3.3.2. X-Ray Diffraction (XRD) Analysis

The XRD overlay on Fig. 3.5 shows the difference of F1 and F2 PM and extruded sample. It is clear that the extruded sample become amorphous compared to the PM.

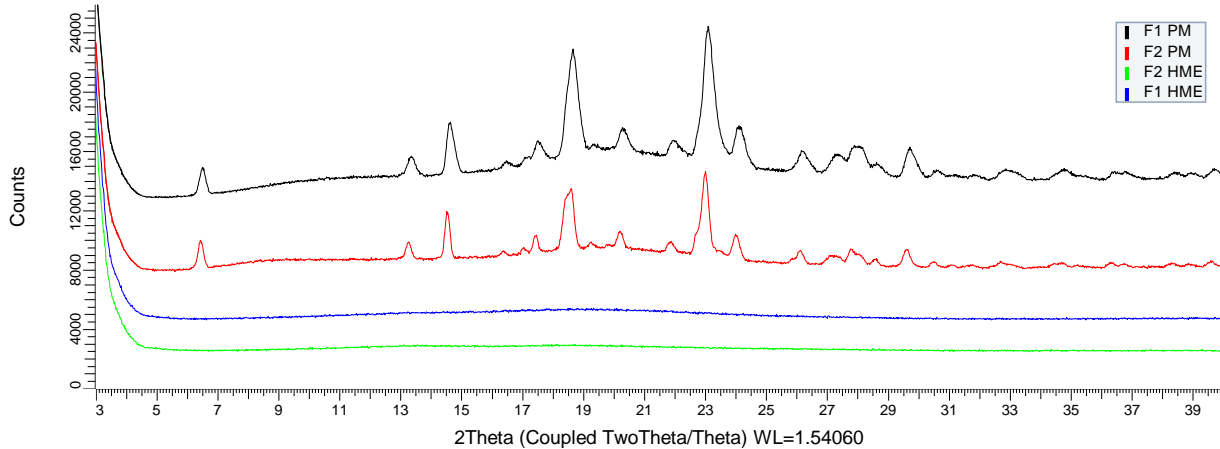


Figure 3.5. XRD overlay of F1 and F2.

3.3.3. Filament Texture Analysis

The HME process successfully produced two formulations of ketoprofen-loaded filaments. During 3D printing, the filament is fed automatically at a constant speed through rigid feeding gear, and the gear will easily break the filament. To fit the 3D printer's requirement, the filaments must have desirable properties to work in the feeding system. The material properties that are hard in general and difficult to bend are regarded as high stiffness, indicating low ductility [75]. The extruded filaments' stiffness travel distance and stress properties were adjusted and evaluated, along with the PLA material as the reference for the printability properties. As shown in Table 3.3, both F1 and F2 demonstrated adequate mechanical properties (successfully printed ten times each) and appeared to have very similar and comparable characteristics with commercial PLA filament products. In this case, the TA test demonstrates the production of the successful filaments for 3D printing by hot-melt extrusion.

Table 3.3. Filament's stiffness test results.

Formulations	Force (g)	Distance (mm)	Stress (g/mm ²)	Stiffness (g/mm)	Property
PLA	1189±12.62	3.75±0.21	10825.054±366.197	317.6±14.71	adequate
F1	628.78±25.49	8.57±0.96	6933.691±974.492	73.36±28.01	adequate
F2	431.5±9.44	6.8±0.45	7006.152±434.166	63.46±11.23	adequate

3.3.4. Tablets Morphology Analysis

The core and shell cross-section of 3D-printed tablets SEM pictures showed that the tablets are smooth and have clear layer by layer FDM printing performance. Figure 3.6 also proved the difference between the 3D printing densities microscopically. The outside shell looked porous and loose, but the structure was much tighter than the inside core. The layer-by-layer printing style can also be seen in the bottom left SEM picture (Figure 3.5).

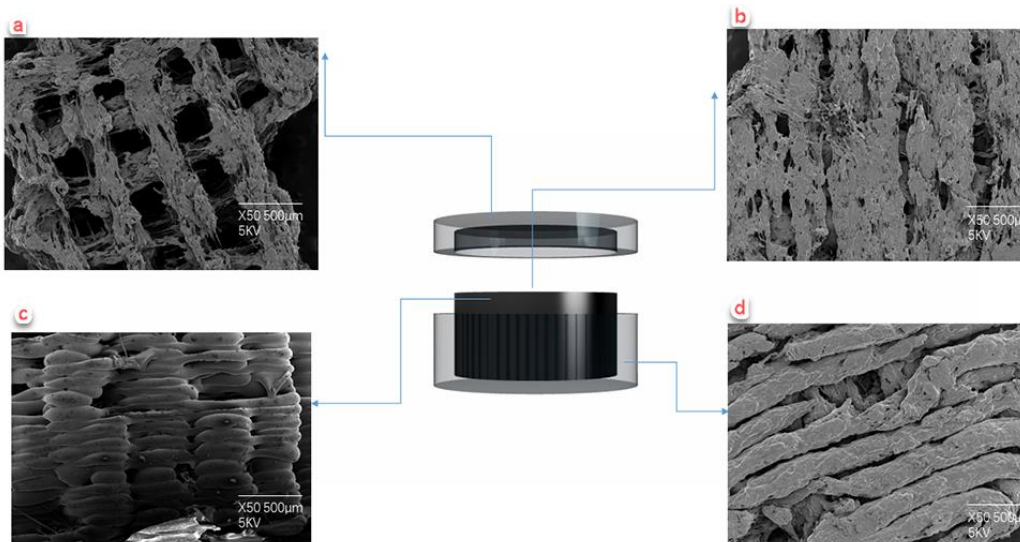


Figure 3.6. SEM 3D structure of T5, with a 30% shell fill and 50% core fill, (a) top view of the shell (b) top view of the core (c) side view of the core, and (d) side view of the shell.

The geometric characteristics for 3D printed tablets data (Table 3.4) showed consistency in size, shape, and quality, thus indicating uniformity in the production of tablets by the FDM 3D printing technique. From the hardness data (Table 3.4 **Error! Reference source not found.**), due to the structured design of the tablet's shell core, its hardness mainly depends on the shell's density and is independent of the core; hardness would increase with an increase in the shell density.

Table 3.4. Geometric characteristics and textural properties of the 3D printed tablets.

Tablets	Diameter(mm)	Height(mm)	Weight(mg)	Hardness (Kp)
20%Shell 40%Core (T1)	10.04±0.17	5.07±0.08	337±24	14.4±0.1
20%Shell 50%Core (T2)	10.14±0.32	5.05±0.09	339±30	14.4±0.1
20%Shell 60%Core (T3)	10.08±0.28	5.02±0.05	347±12	14.4±0.1
30%Shell 40%Core (T4)	10.09±0.31	5.11±0.21	332±17	15.3±0.1
30%Shell 50%Core (T5)	9.98±0.23	5.02±0.06	340±12	15.1±0.2
30%Shell 60%Core (T6)	10.17±0.29	5.17±0.08	351±10	15.1±0.2

40%Shell 40%Core (T7)	10.01±0.09	5.04±0.19	343±18	15.3±0.3
40%Shell 50%Core (T8)	10.05±0.13	5.12±0.25	357±21	15.4±0.2
40%Shell 60%Core (T9)	10.05±0.17	5.15±0.03	347±19	15.4±0.2

3.3.5. *In Vitro Drug Release Study*

Figure 3.7 shows the impact of the infill density for the 3D printed tablets on the drug dissolution performance. The release rate of 3D-printed formulations was slower when the shell and core density increased. Due to the low fill density, the 20% shell infill allows the tablet's core to hydrate, resulting in quicker hydration and better drug release. On the other hand, the 40% infill shell density showed slower drug release profiles. In this study, the 20% shell and 40% core showed a better dissolution rate compared to the other eight density designs.

It is also clear from the dissolution curve that density is one of the critical factors in determining the dissolution rate of 3D printed tablets. 3D printing requires only the change of the software's parameters to make the operation simple, fast, and intuitive, making the process more controllable and conducive to manufacturing personalized designs.

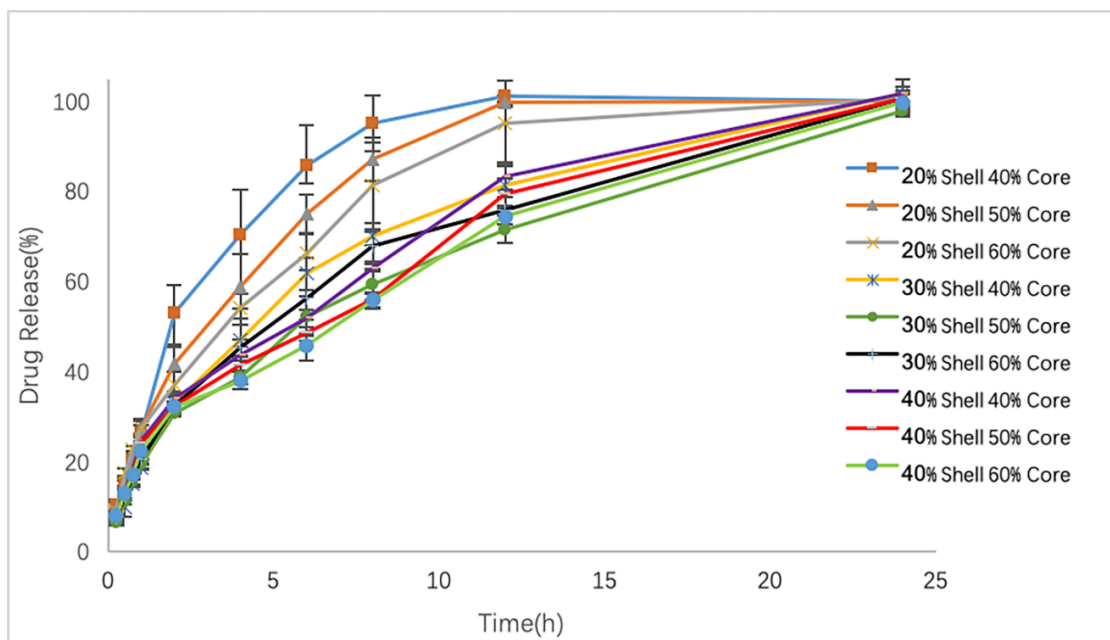


Figure 3.7. In vitro drug release profiles of tablets T1-T9.

3.3.6. Analysis of the Drug Release Using Mathematical Models

In this study, the linear and non-linear curve fitting were conducted by OriginPro 2018 64bit for the different kinetic release models. OriginPro 2018 64bit software can perform a variety of complex data simulations, numerical analyses, and drawing operations. Since the software directly obtains an intuitive release curve from the initial data, it can observe the extensive dispersion data and eliminate the experimental error.

The drug diffusion mechanism can be divided into Fickian and non-Fickian diffusion. When the drug only has Fickian diffusion, the drug's release rate is independent of the drug's concentration, and the concentration is only time-dependent with distance.

0 shows the zero-order kinetic release model (1), first-order kinetic release model (2), Higuchi model (3), Ritger-Peppas model (4), and Peppas-Sahlin model (5) fitting results. From Table 5,

the Ritger-Peppas, Higuchi, and Peppas-Sahlin models fit the dissolution profile better than the other models ($R^2 > 0.95$) [76].

Although the Higuchi model is usually considered the most frequently used model in controlled release drug mathematical model fitting, researchers have also pointed out that the Higuchi model is more suitable for ideal conditions. The drug release for Higuchi model fitting needs to meet the following requirements [67, 77]: The initial drug concentration should be much higher than the solubility limit of the drug. The drug spread is one-dimensional and focused more on when the drug release is under pure diffusion control. The Higuchi model did not count the swelling or dissolution of the polymer carrier.

Based on these prerequisites, the Higuchi model is not appropriate for this study in vitro release of 3D-printed formulations. Since the 3D-printed tablet, in this case, has a unique core-shell structure and the diffusion is not one-dimensional, the initial drug concentration is not much higher than the drug's solubility. The swelling also happened because the HPMCAS HG polymer has the skeleton erosion performance. Though the Higuchi model R^2 fits right here, it may not be applicable to describe this release profile.

Table 3.5. Dissolution kinetic parameters of 3D printing tablets.

	Zero-order		First-order		Ritger-Peppas		Higuchi		Peppas-Sahlin			
	K_0	R^2	K_1	R^2	n	R^2	K_H	R^2	K_1	K_2	N_1	R^2
T1	4.22	0.83	0.31	0.96	0.47	0.97	23.23	0.94	0.19	0.07	0.85	1.00
T2	4.54	0.87	0.29	0.95	0.52	0.97	23.97	0.97	0.18	0.05	0.72	1.00

T3	5.21	0.69	0.42	0.94	0.56	0.96	25.18	0.96	0.11	0.04	0.80	0.99
T4	5.38	0.71	0.26	0.95	0.59	0.96	22.79	0.98	0.12	0.05	0.67	1.00
T5	10.30	0.87	0.51	0.94	0.66	0.98	25.24	1.00	0.11	0.02	0.67	1.00
T6	4.69	0.81	0.32	0.95	0.54	0.97	21.30	0.99	0.13	0.02	0.59	1.00
T7	4.91	0.87	0.19	0.94	0.50	0.96	20.03	0.99	0.12	0.06	0.53	1.00
T8	5.68	0.78	0.50	0.93	0.59	0.94	21.39	0.97	0.10	0.04	0.52	0.99
T9	5.69	0.78	0.49	0.93	0.58	0.94	21.42	0.97	0.09	0.04	0.52	0.99
R ²		0.80		0.94		0.96			0.97			0.99

The Ritger-Peppas equation also demonstrated the drug's release mechanism. When $n \leq 0.45$, it indicates that the drug release is only driven by Fickian diffusion (release rate is independent of the drug concentration). When $n \geq 0.89$, the drug release is more likely driven by case II transport (skeletal erosion and swelling), and when $0.45 < n < 0.89$, the drug release mechanism is called non-Fick diffusion (anomalous transport). The tablets' relevant results are confined to $0.45 < n < 0.89$, indicating that this drug dissolution mechanism has Fickian diffusion and Case II transport [73].

To better judge which diffusion dominated in the ketoprofen-based 3D printed tablets, the Peppas-Sahlin model was introduced here for further calculation. The model considered both Fickian diffusion (the first term of the equation) and the Case II relaxation (the second term of the equation) contribution. The following formula can calculate the percentage of drugs released by Fickian diffusion (F):

$$F = 1/(1 + K_2/K_1 t^{n_1}) \quad (7)$$

The ratio of case II relaxation (R) to F can be calculated by the following formula [78, 79]:

$$\frac{R}{F} = k_2/k_1 t^{n_1} \quad (8)$$

Table 6. R/F parameters for T1-T9 fitted by Peppas-Sahlin model.

	T1	T2	T3	T4	T5	T6	T7	T8	T9
R/F	1.69	1.52	1.50	1.29	1.21	1.13	1.38	1.20	1.07

Table 3.6 showed that the R/F of all nine different density tablets is more significant than 1, so case II relaxation dominates the dissolution part compared to Fickian diffusion. It can also conclude that its dominant position will gradually weaken as the density increases.

Furthermore, it can be seen from Table 6 that the Peppas-Sahlin model ($R^2=0.99$) fits best in comparison to R^2 . This selected model can be used to describe the mechanism of drug release from the polymeric systems, and this study is considered dominated by case II relaxation drug release mechanism. This equation can accurately predict the release rate and diffusion mechanism of the 3D printed dosage forms in this study, which is significant for future research.

3.4. Conclusions

Through this research, many ketoprofen-loaded filaments (30% w/w) were successfully produced using HME and printed as tablets made with different density geometries and formulations. This aspect of the research suggested that the materials used significantly improved their dissolution rate after the HME and 3D printing process. The present findings also confirmed that the printing density greatly influenced 3D printed tablets' dissolution rate. When the density is greater, the dissolution is slower.

References

1. Leuner, C., & Dressman, J. (2000). Improving drug solubility for oral delivery using solid dispersions. *European journal of Pharmaceutics and Biopharmaceutics*, 50(1), 47-60. [https://doi.org/10.1016/s0939-6411\(00\)00076-x](https://doi.org/10.1016/s0939-6411(00)00076-x).
2. Repka, M. A., Bandari, S., Kallakunta, V. R., Vo, A. Q., McFall, H., Pimparade, M. B., & Bhagurkar, A. M. (2018). Melt extrusion with poorly soluble drugs—An integrated review. *International journal of pharmaceutics*, 535(1-2), 68-85. <https://doi.org/10.1016/j.ijpharm.2017.10.056>.
3. Yu, L. (2001). Amorphous pharmaceutical solids: preparation, characterization and stabilization. *Advanced drug delivery reviews*, 48(1), 27-42. [https://doi.org/10.1016/s0169-409x\(01\)00098-9](https://doi.org/10.1016/s0169-409x(01)00098-9).
4. Vasconcelos, T., Sarmiento, B., & Costa, P. (2007). Solid dispersions as strategy to improve oral bioavailability of poor water soluble drugs. *Drug discovery today*, 12(23-24), 1068-1075. <https://doi.org/10.1016/j.drudis.2007.09.005>.
5. Hancock, B. C., & Parks, M. (2000). What is the true solubility advantage for amorphous pharmaceuticals?. *Pharmaceutical research*, 17(4), 397-404. <https://doi.org/10.1023/a:1007516718048>.
6. Brouwers, J., Brewster, M. E., & Augustijns, P. (2009). Supersaturating drug delivery systems: the answer to solubility-limited oral bioavailability?. *Journal of pharmaceutical sciences*, 98(8), 2549-2572. <https://doi.org/10.1002/jps.21650>.
7. Abu-Diak, O. A., Jones, D. S., & Andrews, G. P. (2011). An investigation into the dissolution properties of celecoxib melt extrudates: understanding the role of polymer

8. type and concentration in stabilizing supersaturated drug concentrations. *Molecular pharmaceutics*, 8(4), 1362-1371. <https://doi.org/10.1021/mp200157b>.
9. Serajuddin, A. T. (1999). Solid dispersion of poorly water-soluble drugs: Early promises, subsequent problems, and recent breakthroughs. *Journal of pharmaceutical sciences*, 88(10), 1058-1066. <https://doi.org/10.1021/js980403l>.
10. Shanbhag, A., Rabel, S., Nauka, E., Casadevall, G., Shivanand, P., Eichenbaum, G., & Mansky, P. (2008). Method for screening of solid dispersion formulations of low-solubility compounds—miniaturization and automation of solvent casting and dissolution testing. *International journal of pharmaceutics*, 351(1-2), 209-218. <https://doi.org/10.1016/j.ijpharm.2007.09.042>.
11. Zheng, W., Jain, A., Papoutsakis, D., Dannenfelser, R. M., Panicucci, R., & Garad, S. (2012). Selection of oral bioavailability enhancing formulations during drug discovery. *Drug development and industrial pharmacy*, 38(2), 235-247. <https://doi.org/10.3109/03639045.2011.602406>.
12. Marsac, P. J., Shamblin, S. L., & Taylor, L. S. (2006). Theoretical and practical approaches for prediction of drug–polymer miscibility and solubility. *Pharmaceutical research*, 23(10), 2417-2426. <https://doi.org/10.1007/s11095-006-9063-9>.
13. Abu-Diak, O. A., Jones, D. S., & Andrews, G. P. (2012). Understanding the performance of melt-extruded poly (ethylene oxide)–bicalutamide solid dispersions: characterisation of microstructural properties using thermal, spectroscopic and drug release methods. *Journal of pharmaceutical sciences*, 101(1), 200-213. <https://doi.org/10.1002/jps.22748>.
14. Gupta, J., Nunes, C., Vyas, S., & Jonnalagadda, S. (2011). Prediction of solubility parameters and miscibility of pharmaceutical compounds by molecular dynamics

simulations. *The Journal of Physical Chemistry B*, 115(9), 2014-2023.

<https://doi.org/10.1021/jp108540n>.

15. Marsac, P. J., Li, T., & Taylor, L. S. (2009). Estimation of drug–polymer miscibility and solubility in amorphous solid dispersions using experimentally determined interaction parameters. *Pharmaceutical research*, 26(1), 139-151. <https://doi.org/10.1007/s11095-008-9721-1>.
16. Paudel, A., Van Humbeeck, J., & Van den Mooter, G. (2010). Theoretical and experimental investigation on the solid solubility and miscibility of naproxen in poly(vinylpyrrolidone). *Molecular pharmaceutics*, 7(4), 1133-1148. <https://doi.org/10.1021/mp100013p>.
17. Tao, J., Sun, Y., Zhang, G. G., & Yu, L. (2009). Solubility of small-molecule crystals in polymers: D-mannitol in PVP, indomethacin in PVP/VA, and nifedipine in PVP/VA. *Pharmaceutical research*, 26(4), 855-864. <https://doi.org/10.1007/s11095-008-9784-z>.
18. Sun, Y. E., Tao, J., Zhang, G. G., & Yu, L. (2010). Solubilities of crystalline drugs in polymers: an improved analytical method and comparison of solubilities of indomethacin and nifedipine in PVP, PVP/VA, and PVAc. *Journal of pharmaceutical sciences*, 99(9), 4023-4031. <https://doi.org/10.1002/jps.22251>.
19. Caron, V., Tajber, L., Corrigan, O. I., & Healy, A. M. (2011). A comparison of spray drying and milling in the production of amorphous dispersions of sulfathiazole/polyvinylpyrrolidone and sulfadimidine/polyvinylpyrrolidone. *Molecular pharmaceutics*, 8(2), 532-542. <https://doi.org/10.1021/mp1003674>.

20. Rubinstein, M. (2010). Polymer physics—The ugly duckling story: will polymer physics ever become a part of “proper” physics?. *Journal of Polymer Science Part B: Polymer Physics*, 48(24), 2548-2551. <https://doi.org/10.1002/polb.22135>.
21. Lin, D., & Huang, Y. (2010). A thermal analysis method to predict the complete phase diagram of drug–polymer solid dispersions. *International journal of pharmaceutics*, 399(1-2), 109-115. <https://doi.org/10.1016/j.ijpharm.2010.08.013>.
22. Hoesi, Y., Yamaura, K., & Matsuzawa, S. (1992). A lattice treatment of crystalline solvent-amorphous polymer mixtures on melting point depression. *The Journal of Physical Chemistry*, 96(26), 10584-10586. <https://doi.org/10.1021/j100205a002>.
23. Silva, M. A., De Paoli, M. A., & Felisberti, M. I. (1998). Flory-Huggins interaction parameter of poly (ethylene oxide)/poly (epichlorohydrin) and poly (ethylene oxide)/poly (epichlorohydrin-co-ethylene oxide) blends. *Polymer*, 39(12), 2551-2556. [https://doi.org/10.1016/S0032-3861\(97\)00574-0](https://doi.org/10.1016/S0032-3861(97)00574-0).
24. Moseson, D. E., & Taylor, L. S. (2018). The application of temperature-composition phase diagrams for hot melt extrusion processing of amorphous solid dispersions to prevent residual crystallinity. *International journal of pharmaceutics*, 553(1-2), 454-466. <https://doi.org/10.1016/j.ijpharm.2018.10.055>.
25. Baird, J. A., Van Eerdenbrugh, B., & Taylor, L. S. (2010). A classification system to assess the crystallization tendency of organic molecules from undercooled melts. *Journal of pharmaceutical sciences*, 99(9), 3787-3806. <https://doi.org/10.1002/jps.22197>.
26. Blaabjerg, L. I., Lindenberg, E., Löbmann, K., Grohganz, H., & Rades, T. (2016). Glass forming ability of amorphous drugs investigated by continuous cooling and isothermal

transformation. *Molecular pharmaceutics*, 13(9), 3318-3325.

<https://doi.org/10.1021/acs.molpharmaceut.6b00650>.

27. Just, S., Sievert, F., Thommes, M., & Breitzkreutz, J. (2013). Improved group contribution parameter set for the application of solubility parameters to melt extrusion. *European Journal of Pharmaceutics and Biopharmaceutics*, 85(3), 1191-1199.

<https://doi.org/10.1016/j.ejpb.2013.04.006>.

28. Forster, A., Hemenstall, J., Tucker, I., & Rades, T. (2001). Selection of excipients for melt extrusion with two poorly water-soluble drugs by solubility parameter calculation and thermal analysis. *International journal of pharmaceutics*, 226(1-2), 147-161.

[https://doi.org/10.1016/S0378-5173\(01\)00801-8](https://doi.org/10.1016/S0378-5173(01)00801-8).

29. Barton, A. F. (2017). *CRC handbook of solubility parameters and other cohesion parameters*. Routledge.

30. Bhugra, C., & Pikal, M. J. (2008). Role of thermodynamic, molecular, and kinetic factors in crystallization from the amorphous state. *Journal of pharmaceutical sciences*, 97(4), 1329-1349. <https://doi.org/10.1002/jps.21138>.

31. Li, S., Tian, Y., Jones, D. S., & Andrews, G. P. (2016). Optimising drug solubilisation in amorphous polymer dispersions: rational selection of hot-melt extrusion processing parameters. *Aaps Pharmscitech*, 17(1), 200-213. <https://doi.org/10.1208/s12249-015-0450-6>.

32. Newman, A., Knipp, G., & Zografi, G. (2012). Assessing the performance of amorphous solid dispersions. *Journal of pharmaceutical sciences*, 101(4), 1355-1377.

<https://doi.org/10.1002/jps.23031>.

33. Leuner, C., & Dressman, J. (2000). Improving drug solubility for oral delivery using solid dispersions. *European journal of Pharmaceutics and Biopharmaceutics*, 50(1), 47-60. [https://doi.org/10.1016/s0939-6411\(00\)00076-x](https://doi.org/10.1016/s0939-6411(00)00076-x).
34. Vasconcelos, T., Sarmiento, B., & Costa, P. (2007). Solid dispersions as strategy to improve oral bioavailability of poor water soluble drugs. *Drug discovery today*, 12(23-24), 1068-1075. <https://doi.org/10.1016/j.drudis.2007.09.005>.
35. Yu, L. (2001). Amorphous pharmaceutical solids: preparation, characterization and stabilization. *Advanced drug delivery reviews*, 48(1), 27-42. [https://doi.org/10.1016/s0169-409x\(01\)00098-9](https://doi.org/10.1016/s0169-409x(01)00098-9).
36. He, Y., & Ho, C. (2015). Amorphous solid dispersions: utilization and challenges in drug discovery and development. *Journal of pharmaceutical sciences*, 104(10), 3237-3258. <https://doi.org/10.1002/jps.24541>.
37. Brouwers, J., Brewster, M. E., & Augustijns, P. (2009). Supersaturating drug delivery systems: the answer to solubility-limited oral bioavailability?. *Journal of pharmaceutical sciences*, 98(8), 2549-2572. <https://doi.org/10.1002/jps.21650>.
38. Hancock, B. C., & Parks, M. (2000). What is the true solubility advantage for amorphous pharmaceuticals?. *Pharmaceutical research*, 17(4), 397-404. <https://doi.org/10.1023/a:1007516718048>.
39. Repka, M. A., Bandari, S., Kallakunta, V. R., Vo, A. Q., McFall, H., Pimparade, M. B., & Bhagurkar, A. M. (2018). Melt extrusion with poorly soluble drugs—An integrated review. *International journal of pharmaceutics*, 535(1-2), 68-85. <https://doi.org/10.1016/j.ijpharm.2017.10.056>.

40. Patil, H., Tiwari, R. V., & Repka, M. A. (2016). Hot-melt extrusion: from theory to application in pharmaceutical formulation. *Aaps Pharmscitech*, 17(1), 20-42.
<https://doi.org/10.1208/s12249-015-0360-7>.
41. Zhang, J., Feng, X., Patil, H., Tiwari, R. V., & Repka, M. A. (2017). Coupling 3D printing with hot-melt extrusion to produce controlled-release tablets. *International journal of pharmaceutics*, 519(1-2), 186-197.
<https://doi.org/10.1016/j.ijpharm.2016.12.049>.
42. Bandaranayake, W. M. (2006). Quality control, screening, toxicity, and regulation of herbal drugs. *Modern phytomedicine: turning medicinal plants into drugs*, 25-57.
<https://doi.org/10.1016/j.trac.2016.02.001>.
43. Zhang, L., & Mao, S. (2017). Application of quality by design in the current drug development. *Asian journal of pharmaceutical sciences*, 12(1), 1-8.
<https://doi.org/10.1016/j.ajps.2016.07.006>.
44. Saini, M., Tripathy, S., & Dureja, H. (2014). USA FDA's implementation of QbD and GDUFA: A wakeup call for other regulatory agencies across the globe. *Journal of Medical Marketing*, 14(2-3), 108-114. <https://doi.org/10.1177/1745790414564259>.
45. Fukuda, I. M., Pinto, C. F. F., Moreira, C. D. S., Saviano, A. M., & Lourenço, F. R. (2018). Design of experiments (DoE) applied to pharmaceutical and analytical quality by design (QbD). *Brazilian Journal of Pharmaceutical Sciences*, 54.
<https://doi.org/10.1590/s2175-97902018000001006>.
46. N. Politis, S., Colombo, P., Colombo, G., & M. Rekkas, D. (2017). Design of experiments (DoE) in pharmaceutical development. *Drug development and industrial pharmacy*, 43(6), 889-901. <https://doi.org/10.1080/03639045.2017.1291672>.

47. Suwardie, H., Wang, P., Todd, D. B., Panchal, V., Yang, M., & Gogos, C. G. (2011). Rheological study of the mixture of acetaminophen and polyethylene oxide for hot-melt extrusion application. *European journal of pharmaceutics and biopharmaceutics*, 78(3), 506-512. <https://doi.org/10.1016/j.ejpb.2011.03.013>.
48. Ma, X., Huang, S., Lowinger, M. B., Liu, X., Lu, X., Su, Y., & Williams III, R. O. (2019). Influence of mechanical and thermal energy on nifedipine amorphous solid dispersions prepared by hot melt extrusion: Preparation and physical stability. *International journal of pharmaceutics*, 561, 324-334. <https://doi.org/10.1016/j.ijpharm.2019.03.014>.
49. Tian, Y., Booth, J., Meehan, E., Jones, D. S., Li, S., & Andrews, G. P. (2013). Construction of drug–polymer thermodynamic phase diagrams using Flory–Huggins interaction theory: identifying the relevance of temperature and drug weight fraction to phase separation within solid dispersions. *Molecular pharmaceutics*, 10(1), 236-248. <https://doi.org/10.1021/mp300386v>.
50. Suwardie, H., Wang, P., Todd, D. B., Panchal, V., Yang, M., & Gogos, C. G. (2011). Rheological study of the mixture of acetaminophen and polyethylene oxide for hot-melt extrusion application. *European journal of pharmaceutics and biopharmaceutics*, 78(3), 506-512. <https://doi.org/10.1016/j.ejpb.2011.03.013>.
51. Kyeremateng, S. O., Pudlas, M., & Woehrle, G. H. (2014). A fast and reliable empirical approach for estimating solubility of crystalline drugs in polymers for hot melt extrusion formulations. *Journal of pharmaceutical sciences*, 103(9), 2847-2858. <https://doi.org/10.1002/jps.23941>.

52. Thakkar, R., Thakkar, R., Pillai, A., Ashour, E. A., & Repka, M. A. (2020). Systematic screening of pharmaceutical polymers for hot melt extrusion processing: A comprehensive review. *International journal of pharmaceutics*, 576, 118989. <https://doi.org/10.1016/j.ijpharm.2019.118989>.
53. Huang, Y., & Dai, W. G. (2014). Fundamental aspects of solid dispersion technology for poorly soluble drugs. *Acta Pharmaceutica Sinica B*, 4(1), 18-25. <https://doi.org/10.1016/j.apsb.2013.11.001>.
54. Kipping, T., & Rein, H. (2013). A new method for the continuous production of single dosed controlled release matrix systems based on hot-melt extruded starch: Analysis of relevant process parameters and implementation of an in-process control. *European Journal of Pharmaceutics and Biopharmaceutics*, 84(1), 156-171. <https://doi.org/10.1016/j.ejpb.2012.12.013>.
55. Tiwari, Roshan V., Hemlata Patil, and Michael A. Repka. "Contribution of hot-melt extrusion technology to advance drug delivery in the 21st century." *Expert opinion on drug delivery* 13.3 (2016): 451-464, <https://doi.org/10.1517/17425247.2016.1126246>.
56. Repka, Michael A., et al. "Applications of hot-melt extrusion for drug delivery." *Expert opinion on drug delivery* 5.12 (2008): 1357-1376, <https://doi.org/10.1517/17425240802583421>.
57. Vasconcelos, Teofilo, Bruno Sarmiento, and Paulo Costa. "Solid dispersions as strategy to improve oral bioavailability of poor water soluble drugs." *Drug discovery today* 12.23-24 (2007): 1068-1075, <https://doi.org/10.1016/j.drudis.2007.09.005>.

58. Sareen, Swati, George Mathew, and Lincy Joseph. "Improvement in solubility of poor water-soluble drugs by solid dispersion." *International journal of pharmaceutical investigation* 2.1 (2012): 12, <http://doi.org/10.4103/2230-973X.96921>.
59. Goyanes, Alvaro, et al. "Fabrication of controlled-release budesonide tablets via desktop (FDM) 3D printing." *International journal of pharmaceutics* 496.2 (2015): 414-420, <https://doi.org/10.1016/j.ijpharm.2015.10.039>.
60. Zhang, Jiayang, et al. "Coupling 3D printing with hot-melt extrusion to produce controlled-release tablets." *International journal of pharmaceutics* 519.1-2 (2017): 186-197, <https://doi.org/10.1016/j.ijpharm.2016.12.049>.
61. Melocchi, Alice, et al. "Hot-melt extruded filaments based on pharmaceutical grade polymers for 3D printing by fused deposition modeling." *International journal of pharmaceutics* 509.1-2 (2016): 255-263, <https://doi.org/10.1016/j.ijpharm.2016.05.036>.
62. Trenfield, Sarah J., et al. "3D printed drug products: Non-destructive dose verification using a rapid point-and-shoot approach." *International journal of pharmaceutics* 549.1-2 (2018): 283-292, <https://doi.org/10.1016/j.ijpharm.2020.119066>.
63. Gültekin, Hazal Ezgi, Serdar Tort, and Füsün Acartürk. "An effective technology for the development of immediate release solid dosage forms containing low-dose drug: fused deposition modeling 3D printing." *Pharmaceutical research* 36.9 (2019): 1-13, <https://doi.org/10.1007/s11095-019-2655-y>.
64. Gioumouxouzis, Christos I., et al. "3D printed oral solid dosage forms containing hydrochlorothiazide for controlled drug delivery." *Journal of Drug Delivery Science and Technology* 40 (2017): 164-171, <https://doi.org/10.1016/j.jddst.2017.06.008>.

65. Goole, Jonathan, and Karim Amighi. "3D printing in pharmaceuticals: A new tool for designing customized drug delivery systems." *International journal of pharmaceuticals* 499.1-2 (2016): 376-394, <https://doi.org/10.1016/j.ijpharm.2015.12.071>.
66. Jamróz, Witold, et al. "3D printing in pharmaceutical and medical applications—recent achievements and challenges." *Pharmaceutical research* 35.9 (2018): 176, <https://doi.org/10.1007/s11095-018-2454-x>.
67. Tsume, Yasuhiro, et al. "In silico prediction of drug dissolution and absorption with variation in intestinal pH for BCS class II weak acid drugs: ibuprofen and ketoprofen." *Biopharmaceutics & drug disposition* 33.7 (2012): 366-377, <https://doi.org/10.1002/bdd.1800>.
68. Siepmann, J., and A. Göpferich. "Mathematical modeling of bioerodible, polymeric drug delivery systems." *Advanced drug delivery reviews* 48.2-3 (2001): 229-247, [https://doi.org/10.1016/S0169-409X\(01\)00116-8](https://doi.org/10.1016/S0169-409X(01)00116-8).
69. Costa, P., and J. M. Sousa Lobo. "Evaluation of mathematical models describing drug release from estradiol transdermal systems." *Drug development and industrial pharmacy* 29.1 (2003): 89-97, <https://doi.org/10.1081/DDC-120016687>.
70. Varelas, Charalambos G., David G. Dixon, and Carol A. Steiner. "Zero-order release from biphasic polymer hydrogels." *Journal of controlled release* 34.3 (1995): 185-192, [https://doi.org/10.1016/0168-3659\(94\)00085-9](https://doi.org/10.1016/0168-3659(94)00085-9).
71. Sweeney, Jerry J., and Alan K. Burnham. "Evaluation of a simple model of vitrinite reflectance based on chemical kinetics." *AAPG bulletin* 74.10 (1990): 1559-1570, <https://doi.org/10.1306/0C9B251F-1710-11D7-8645000102C1865D>.

72. Gohel, Mukesh C., Maulik K. Panchal, and Viral V. Jogani. "Novel mathematical method for quantitative expression of deviation from the Higuchi model." *Aaps Pharmscitech* 1.4 (2000): 43-48, <https://doi.org/10.1208/pt010431>.
73. Petropoulos, George P., Kostas Arvanitis, and Nick Sigrimis. "Hyperion hyperspectral imagery analysis combined with machine learning classifiers for land use/cover mapping." *Expert systems with Applications* 39.3 (2012): 3800-3809, <https://doi.org/10.1016/j.eswa.2011.09.083>.
74. Ritger, Philip L., and Nikolaos A. Peppas. "A simple equation for description of solute release I. Fickian and non-fickian release from non-swellable devices in the form of slabs, spheres, cylinders or discs." *Journal of controlled release* 5.1 (1987): 23-36, [https://doi.org/10.1016/0168-3659\(87\)90034-4](https://doi.org/10.1016/0168-3659(87)90034-4).
75. Mathematical models of drug release. (2015). *Strategies to Modify the Drug Release from Pharmaceutical Systems*, 63–86, <https://doi.org/10.1016/B978-0-08-100092-2.00005-9>.
76. Rösler, Joachim, Harald Harders, and Martin Bäker. *Mechanical behaviour of engineering materials: metals, ceramics, polymers, and composites*. Springer Science & Business Media, 2007, <https://doi.org/10.1007/978-3-540-73448-2>.
77. Costa, Paulo, and Jose Manuel Sousa Lobo. "Modeling and comparison of dissolution profiles." *European journal of pharmaceutical sciences* 13.2 (2001): 123-133, [https://doi.org/10.1016/S0928-0987\(01\)00095-1](https://doi.org/10.1016/S0928-0987(01)00095-1).
78. Zhang, Jiaxiang, et al. "Hydroxypropyl methylcellulose-based controlled release dosage by melt extrusion and 3D printing: Structure and drug release correlation." *Carbohydrate polymers* 177 (2017): 49-57, <https://doi.org/10.1016/j.carbpol.2017.08.058>.

79. Peppas, Nikolaos A., and Jennifer J. Sahlin. "A simple equation for the description of solute release. III. Coupling of diffusion and relaxation." *International journal of pharmaceutics* 57.2 (1989): 169-172, [https://doi.org/10.1016/0378-5173\(89\)90306-2](https://doi.org/10.1016/0378-5173(89)90306-2).
80. Unagolla, Janitha M., and Ambalangodage C. Jayasuriya. "Drug transport mechanisms and in vitro release kinetics of vancomycin encapsulated chitosan-alginate polyelectrolyte microparticles as a controlled drug delivery system." *European Journal of Pharmaceutical Sciences* 114 (2018): 199-209, <https://doi.org/10.1016/j.ejps.2017.12.012>.

VITA

SKILLS

- Proficiency in characterization method development especially the solid states analysis techniques: PXRD, DSC, TGA, FT-NIR, SEM, PLM, HPLC. Extensive experience in novel or commonly used technologies for drug product development and manufacturing: 3D printing, Hot melt extrusion (HME), Spray drying, single/multiple station tablet compressor.
- Hands on experience in laboratory scale development such as blending, compaction and material science; knowledge in formulation and process development of liquid and solid dosage forms such as solution, suspension, tablet, and capsule. Knowledge of manufacturing processes such as blending, milling, tableting, and coating.
- Skills of Design of Experiment (DoE), Quality by Design (QbD), and statistical analysis (Autodesk®, Materials Studio®, Fusion 360®, Origin Lab, SPSS, Octave). Strong understanding of GMP guidelines and FDA regulations related to the pharmaceutical industry.
- Strong capability of data generation, interpretation, and presentation. Superior cooperative and communication skills of complex data and science.
- Self-motivated learner with the certificate in Python, R, HTML, JavaScript, SQL, MATLAB, Tableau, Data science, Web development and Machine learning.

EDUCATION

08/2019- Present	Ph.D. in Pharmaceutics, University of Mississippi, United States
08/2017- 05/2019	M.S. in Pharmaceutics, University of Mississippi, United States
09/2013- 06/2017	B.S. in Pharmaceutics, China Pharmaceutical University, China

EXPERIENCE

03/2021- Present	Scientist I on Small Molecule Formulation Development at Biogen, Boston, MA
03/2021- 03/2022	Technical Development Intern at Biogen, Boston, MA
08/2018- 03/2021	Research Assistant at University of Mississippi, Oxford, MS
06/2015- 08/2015	Research Intern at Prinbury Bio Pharmaceutical, Shanghai, China

CERTIFICATS

09/2018	Hands-on Course of Tablet Technology
11/2020	Programming for Everybody (Getting Started with Python)
01/2021	Machine Learning by Standard University
01/2021	Business Metrics for Data-Driven Companies
02/2021	Web Developer Bootcamp 2021

PUBLICATIONS

- Wang, M., Li, Y., Srinivasan, P., Hu, Z., Wang, R., Saragih, A., ... & Murthy, S. N. (2018). Interactions Between Biological Products and Product Packaging and Potential Approaches to Overcome Them. *AAPS PharmSciTech*, 1-6

- Submitted Development of Controlled Release Oral Dosages by Density Gradient Modification via 3D Printing and HME Technology to *Journal of Drug Delivery Science and Technology* (JDDST).
- Submitted Prediction and Construction of Drug-Polymer Binary System Thermodynamic Phase Diagram in Amorphous Solid Dispersions (ASDs) to *AAPS PharmSciTech*.

LEADERSHIP ROLES AND ACTIVITIES

11/2019	Presenter at AAPS PharmSci 360 2019
01/2019- Present	Rho Chi member
05/2018- Present	American Association of Pharmaceutical Scientists (AAPS) member
11/2018	Presenter at AAPS PharmSci 360 2018
08/2015-02-2016	Team leader in National College Student Innovation Training Program